

**DEVELOPMENT OF
VIRTUAL TODDLER FIT MODELS FOR
CHILD SAFETY RESTRAINT DESIGN**

**K. HAN KIM, MONICA L.H. JONES
SHEILA M. EBERT, LAURA MALIK,
MIRIAM A. MANARY, MATTHEW P. REED,
KATHLEEN D. KLINICH**



Technical Report Documentation Page

1. Report No. UMTRI-2015-38		2. Government Accession No.		3. Recipient's Catalog No.	
4. Title and Subtitle Development of Virtual Toddler Fit Models for Child Safety Restraint Design			5. Report Date December 2015		
			6. Performing Organization Code		
7. Author(s) Kim, K. Han; Jones, Monica L. H.; Ebert, Sheila M.; Malik, Laura; Manary, Miriam A.; Reed, Matthew P.; and Klinich, Kathleen D.			8. Performing Organization Report No.		
9. Performing Organization Name and Address University of Michigan Transportation Research Institute 2901 Baxter Rd. Ann Arbor MI 48109			10. Work Unit No. (TRAIS)		
			11. Contract or Grant No.		
12. Sponsoring Agency Name and Address National Highway Traffic Safety Administration			13. Type of Report and Period Covered Final, January 2014-April 2015		
			14. Sponsoring Agency Code		
15. Supplementary Notes					
16. Abstract The design of child restraints is guided in part by data on the size and shape of child occupants. This study presents for the first time statistical body shape models for children weighing 9 to 27 kg (20 to 60 lb) in a seated posture relevant to child restraint design. A laboratory study was conducted with 47 child participants, ages 12 to 48 months. Standard anthropometric dimensions were taken and whole-body surface scans were conducted in a range of postures. A three-dimensional coordinate measurement system was used to record body landmarks. The body surface data were analyzed using novel template fitting methods to obtain homologous meshes for each participant in a standardized seated posture. Data from the current study were combined with data from a preceding study to obtain body scans from 68 children. Principal component analysis and regression were used to develop a statistical body shape model (SBSM). The SBSM was exercised to create 18 manikins representing children with long and short torsos at body weights ranging from 20 to 60 lb. These manikins will be useful for assessing child accommodation in restraints. The SBSM can provide guidance for the development of anthropomorphic test devices and computational models of child occupants.					
17. Key Word Child anthropometry, child restraint systems			18. Distribution Statement		
19. Security Classif. (of this report)		20. Security Classif. (of this page)		21. No. of Pages	22. Price

ACKNOWLEDGMENTS

This work was funded by the National Highway Traffic Safety Administration (NHTSA) under cooperative agreement DTNH22-10-H-00288 with the University of Michigan. The opinions expressed herein are those of the authors and do not necessarily represent those of NHTSA. Many people at UMTRI contributed to the success of this project, including Brian Eby for the development of the reconfigurable CRS seating fixture and Kyle Boyle who developed the virtual fit concept. Anne Bonnifas, and Andrew Nikolai assisted with data collection. We would also like to thank the many students who supported the scan data processing effort; specifically, Edward Young, Dylan Zwiers, Trevor Sultana, Andrew Nikolai, Emily Lancaster, Jenine McKoy, and Jackie Miller.

CONTENTS

ACKNOWLEDGEMENTS.....	ii
1. EXECUTIVE SUMMARY.....	4
2. INTRODUCTION.....	5
3. METHODS.....	6
3.1. Overview.....	6
3.2. Standard anthropometry.....	6
3.3. Reconfigurable child restraint seating fixture.....	9
3.4. Seating fixture configurations.....	11
3.5. Laboratory hardseat.....	13
3.6. Whole-body scanning.....	15
3.6.1. Marking landmarks.....	15
3.6.2. Scan postures.....	18
3.7. Protocol.....	27
3.8. Scan data processing.....	28
3.9. Body shape modeling.....	31
3.9.1. Toddler scan dataset.....	31
3.9.2. Reference template.....	33
3.9.3. Skeletal linkage system for template posing.....	35
3.9.4. Morphing and fitting.....	37
3.9.5. Posture standardization.....	38
3.9.6. Bootstrapping for participant-specific template generation.....	39
4. RESULTS.....	41
4.1. Participants.....	41
4.2. Body scan data.....	43
4.3. Development of a statistical body shape model.....	47
4.4. Example application.....	53
5. DISCUSSION.....	56
5.1. Accomplishments.....	56
5.2. Limitations and future work.....	56
6. REFERENCES.....	58
7. APPENDICES.....	60
7.1. APPENDIX A: Standard Anthropometric Measures.....	60
7.2. APPENDIX B: Points Digitized on Scans.....	73
7.3. APPENDIX C: Comparison of Standard Anthropometric Measures Across Postures...76	

1. EXECUTIVE SUMMARY

The design of child restraints is guided in part by data on the size and shape of child occupants. This study presents for the first time statistical body shape models for children weighing 9 to 27 kg (20 to 60 lb.) in a seated posture relevant to child restraint design. A laboratory study was conducted with 47 child participants, ages 12 to 48 months. Standard anthropometric dimensions were taken and whole-body surface scans were conducted in a range of postures. A three-dimensional coordinate measurement system was used to record body landmarks. The body surface data were analyzed using novel template fitting methods to obtain homologous meshes for each participant in a standardized seated posture. Data from the current study were combined with data from a preceding study to obtain body scans from 68 children. Principal component analysis and regression were used to develop a statistical body shape model (SBSM). The SBSM was exercised to create 18 manikins representing children with long and short torsos at body weights ranging from 20 to 60 lb. These manikins will be useful for assessing child accommodation in restraints. The SBSM can provide guidance for the development of anthropomorphic test devices and computational models of child occupants.

2. INTRODUCTION

Child restraint system (CRS) manufacturers specify height and weight limits for their products and test them dynamically with a small set of crash dummies. Most CRS manufactured for the U.S. market are tested using the CRABI 12MO, Hybrid III 3YO, and/or the Hybrid III 6YO ATDs as a representation of typical child body size and shape. The dynamic test procedures of FMVSS 213 ensure that CRS provide adequate protection in a crash for children under the allowable weight limit, but they do not ensure that the physical dimensions of the CRS will accommodate any particular percentage of children within the weight limits.

The design of child restraints for the U.S. market is guided in part by one-dimensional, traditional anthropometric survey data gathered in the 1970s by UMTRI (then the Highway Safety Research Institute). Snyder et al. (1977) obtained standard anthropometric dimensions (lengths, widths, and circumferences) on 4127 children from ages 2 weeks to 18 years. A compilation of summary statistics based on those data by Weber et al. (1985) has been widely used to size child restraints. Recently Pagano et al. (2015) reanalyzed these data together with contemporary measurements to show that trends toward higher body weight have likely led to greater child breadth dimensions even in the toddler years.

The development of ATDs and other surrogates for children for dynamic testing has been based almost entirely on traditional anthropometric measures, such as those from Snyder et al. (1977). For example, Irwin and Mertz (1997) presented the anthropometric specifications for the CRABI and Hybrid-III child ATDs. The body dimensions are derived from Snyder et al. (1977) via Weber et al. (1985). Some body shape information was derived from three-dimensional body forms developed by Reynolds et al. (1976) representing three- and six-year-old children. However, these body forms were not based on three-dimensional measurements, but rather were constructed manually to match target lengths, widths, and circumferences. Reed et al. (2000) developed a three-dimensional model of a six-year-old child using surface measurements from a single child scaled to match target dimensions and landmark locations.

Recently, Park and Reed (2015) published the first statistical model of child body shape based on whole-body surface measurements. Whole-body laser scan data from 137 children ages 3 to 11 years in a standing posture were analyzed to create a parametric model that generates a child body form as a function of stature, erecting sitting height, and body weight (see <http://childshape.org>).

The current project seeks to extend this database of child body shapes down to 12 months of age to obtain data useful in the design and evaluation of CRSs. The objectives are (1) to quantify the three-dimensional anthropometry and body shape of children ages 1 to 4 using laser scanning and 3D coordinate measurement in a wide range of postures, including supported seated postures relevant to the vehicle environment, and (2) to develop a set of virtual toddler fit models representing a range of child sizes among children aged 1 to 4 years that can be used for CRS design.

3. METHODS

3.1. Overview

The study protocol was approved by the University of Michigan Institutional Review Board (IRB) for Health Behavior and Health Sciences (IRB # HUM00091202). Participants were recruited through online advertisements flyers at child care facilities and pediatrician offices, and word of mouth. The participant changed into test clothing and standard anthropometric measures were taken. Body landmark locations were recorded in a laboratory hardseat. The body shape of each participant was measured in 12 postures using a whole-body laser scanner and specially constructed seating fixture representative of rear-facing and forward-facing child restraints. Joint center locations were estimated using the surface landmarks. Surface landmark locations were extracted from surface scan data in software. Custom software and methods were used to fit a uniform template to the body scan data and to re-pose body scan data into standardized postures. A statistical shape model was developed that predicts body shape, surface landmarks, and joint center locations as a function of age, gender, weight, body mass index, SHS, stature, and erect seating height for an unsupported seated posture.

3.2. Standard Anthropometry

Anthropometric data were gathered from each child to characterize the overall body size and shape. The standard anthropometry measures listed in Table 1 were obtained using manual measurements. Procedures for obtaining manual measures of child anthropometry are outlined in Snyder et al. 1977. Standard anthropometry techniques detailed by Snyder et al. (1977) measure children less than 2 years of age in a supine posture and children over 2 years in a standing posture. During this study, when possible, some of the measurements were taken in standing/seated and supine postures to allow comparisons with values in the literature. Definitions of the standard anthropometric measures are presented in Appendix A. Anthropometric measures obtained from multiple postures provide preliminary data on how these anthropometric measures vary with posture. If child was not cooperative, a subset of measures was taken. An example of measuring knee height and shoulder height in seated and supine postures is illustrated in Figure 1.



Figure 1. Example of knee height and shoulder height measurements in both seated and supine postures.

Table 1. Anthropometric measures

Measurement	Posture		
	Standing	Sitting	Supine
Weight	X*	Alt.	
Stature	X		X
Bideltoid Breadth	X	Alt.	X
Biacromial Breadth	X	Alt.	
Chest Breadth	X	Alt.	Alt.
Waist Breadth at Omphalion Height	X	X	
Waist Depth at Omphalion Height	X		
Shoulder-Elbow Length	X	Alt.	Alt.
Elbow-Fingertip Length	X	Alt.	Alt.
Bispinous Breadth (Bi-ASIS)	X	Alt.	Alt.
Pelvis Breadth	X		Alt.
Pelvis Depth (ASIS to PSIS)	X		Alt.
Chest Depth (On Spine)	X	Alt.	Alt.
Maximum Hip Breadth		X	X
Buttock-Knee Length		X	X
Buttock-Popliteal Length		X	X
Erect Sitting Height		X	X
Seated Eye Height		X	X
Seated Shoulder Height		X	X
Knee Height		X	X
Tragion to Top of Head	Alt.	X	Alt.
Head Breadth	Alt.	X	Alt.
Head Length	Alt.	X	Alt.
Head Circumference	X	Alt.	
Chest Circumference at Axilla	X	Alt.	
Waist Circumference at Omphalion	X		
Maximum Hip Circumference	X		
Thigh Circumference at Gluteal Fold	X		
Maximum Calf Circumference	X	Alt.	
Ankle Circumference above Malleolus	X	Alt.	
Mid Upper Arm Circumference	X	Alt.	
Maximum Forearm Circumference	X	Alt.	
Date of Birth			
Gender			

*X=preferred posture, Alt.=alternate posture

3.3. Reconfigurable Child Restraint Seating Fixture

A reconfigurable seating fixture was fabricated for this study (Figure 2). It was designed to simulate a range of installed rear-facing (RF) and forward-facing (FF) CRS geometry measured in vehicles. The CRS dimensions used to design the adjustable fixture were derived from a previous study of child restraint and vehicle compatibility which documented the position and orientation of 31 different child restraint, installed in 10 vehicles selected to provide a range of manufacturers and body styles, using LATCH according to manufacturers' directions (Klinich et al., 2015). For the current study, the scanned contours and installed orientations of the CRS were analyzed further to identify typical CRS seat cushion and seatback angles in installed RF and FF configurations. CRS cushion angle and seatback angles were observed to range from 20 to 45-degrees and 115 to 135-degrees relative to horizontal respectively. CRS cushion length and seatback height, and maximum width dimensions of the seating area at the shoulders and hip were also extracted. Cushion length was observed to range 200-300 mm, and the lower side supports were found to range 300-400 mm. These measures were used to design the reconfigurable seating fixture that represents a range of installed CRS conditions.

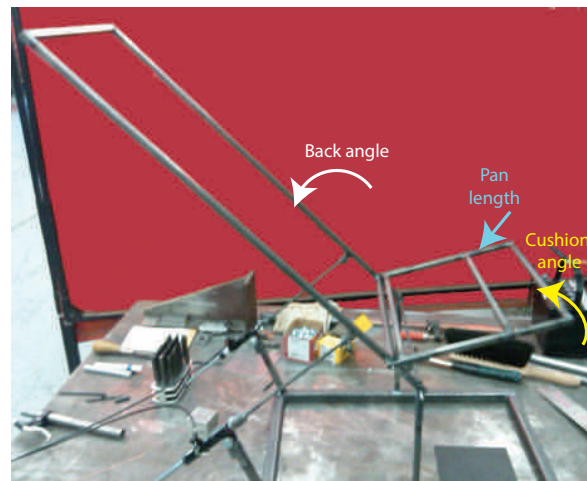


Figure 2. Fabrication of the reconfigurable CRS seating fixture. The seatback and seatpan from are adjustable independently. The seatpan can be adjusted to long and short lengths by removing the front section.

In a study by Ebert et al. (2014), lower extremity postures of toddlers, aged 18-36 months, were recorded in conditions simulating RF and FF child restraints. Analysis of the measured participant postures showed variations in lower extremity posture with child restraint condition. Results of this study informed the design of the reconfigurable seating fixture to incorporate adjustable fixtures to provide sufficient degrees of freedom to position and support the child's lower extremities in a range of postures.

The reconfigurable CRS seating fixture consists of a rigid frame with transparent support surfaces to enable a whole-body laser scanner to capture the toddler's body shape. The fixture design allows clear viewing of the participant's surface anthropometry. The reconfigurable seat was equipped with a 5-point harness, which was fitted and tightened manually to secure the child safely in position. Custom fixtures were fabricated to support the limbs. As shown in Figure 3, vertical poles supported the child's hands so that the arms were abducted and flexed, and foot-

positioning aids supported the child's lower extremity postures. The seatback and seat cushion elements were adjustable in both length and angle.

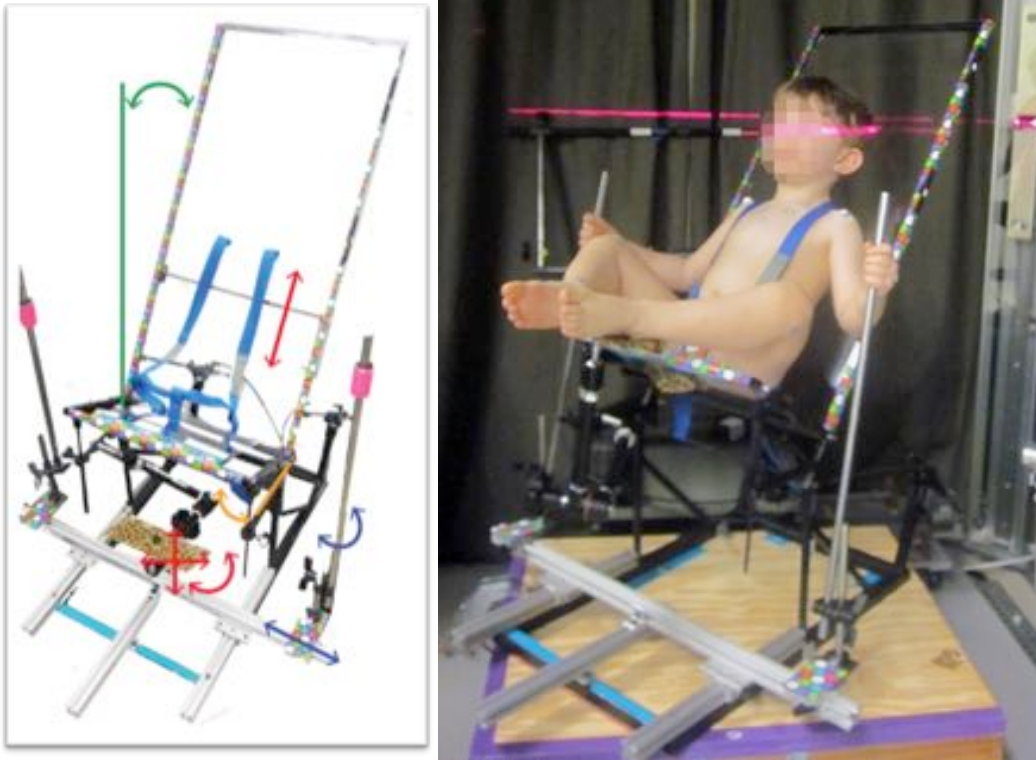


Figure 3. Reconfigurable CRS seating fixture. Adjustability of the fixture indicated by the arrows. Adjustability includes: seatpan length and angle, seatback angle, hand and foot positioning aids. Participant positioned in reconfigurable seating fixture.

Table 2 lists the points on the reconfigurable CRS seating fixture that were recorded in each trial. The recorded points on the harness restraint and the reconfigurable seating fixture were checked to verify that the test conditions were set as intended.

Table 2. Reconfigurable CRS Fixture Point List

Origin
ASIS Left and Right
PSIS Left and Right
CRS Reference Points (4)

3.4. Seating Fixture Configurations

Results from a prior study of lower extremity posture of children in RF and FF CRS (Ebert et al. 2014) were used to identify targeted postures for testing. Five lower extremity postures: relaxed, feet flat, crossed, frog, or elevated accounted for 80% of the postures selected by forward-facing children and 88% of rearward-facing children (Figure 4). Significant differences in the frequencies of posture categories were associated with CRS geometry. In the narrow rear-facing condition, children were most likely to sit in a relaxed posture. With the wide condition, the most common measured posture was feet flat together, with legs splayed more outward. Children more frequently chose a “frog legs” posture with the wider seat. From the general trends with child restraint width, toddlers seem to splay their legs until they are limited by the inner structure of the child restraint. There were no distinct trends with selected posture and the participants’ age or size.



Figure 4. Lower extremity postures recorded in the Toddler Lower Extremity Posture in Child Restraint Systems study (Ebert et al. 2014).

The reconfigurable CRS seating fixture was designed to simulate a range of installed CRS geometry measured in vehicles. Specifically, the included angle between the seatback and seat cushion was set to 90° , and the orientation was varied to represent CRS conditions. Adjustability enabled the fixture to configure in both reclined and upright orientations to represent RF and FF CRS respectively. Pilot testing determined that posture of child participant, nor the quality of the 3D scan data varied meaningfully as a function of the orientation of the seating fixture. Additional evaluation of lower extremity positioning relative to target postures was observed to have minimal effect on the position of a child's torso and pelvis relative to the seating fixture, during both reclined and upright orientations. Therefore, it was determined that children should be tested in the orientation in which they were most comfortable.

For each test condition, the fixture was configured to support the child participants. Upper extremity supports varied to standardized and achieve bilateral symmetrical arm postures position at both 90-degrees to the side and abducted away from torso postures. Lower extremity supports were positioned to vary the hip angles from narrow to wide splay, and set the included knee angles, at acute and obtuse angles.



Figure 5. Child participants seated in reconfigurable fixture in different postures.

3.5. Laboratory Hardseat

The locations of body landmarks were measured using a three-dimensional coordinate measuring machine (FARO Arm®, FARO Technology, USA). The reconfigurable CRS seating fixture was modified to provide access holes to posterior landmarks on the spine and pelvis, such as the posterior-superior iliac spines (PSIS). The seating fixture and its incorporated restraint webbing provided a safe and stable environment to complete the hardseat measures for the toddler participants.

The landmark set and measurement methods were derived from those used in previous studies of automotive posture for both adults and children (Reed et al. 1999, Reed et al. 2005). Posture recorded in the adapted hardseat is shown in Figure 6. Table 3 lists the landmarks recorded in the hardseat. Each of anatomical linkages in the table below were performed separately to reduce the time required to complete, as the children were often very fidgety and had difficulties holding a posture. By design, there was redundancy in digitized anatomical points between the individual linkage segments. The intention was to ensure that points from a linkage could be used to compute an anatomical location recorded in a different linkage, in the event that that child participant was unable to complete the hardseat protocol. For example, relationships between the digitized points on “leg linkage” list were used to predict the pelvis and knee geometry if “all else failed”.



Figure 6. Hardseat

Table 3. Anatomical Hardseat Point List

<p>Pelvis and Seat Origin ASIS Lt and Rt PSIS Lt and Rt CRS Reference Points (4)</p>	<p>Torso Cervicale (C7) Acromion Lt (Anterior) Acromion Lt Marker Suprasternale Chest Triad Markers (3) Substernale Omphalion C7 Marker T4 Marker T8 Marker T12 Marker L3 Marker ASIS Lt and Rt PSIS Lt and Rt</p>	<p>Arm Suprasternale Supsternale Acromion Lt (Anterior) Humeral Epicondyle Medial Lt Humeral Epicondyle Lateral Lt Ulnar Styloid Process Lt Radial Styloid Process Lt</p>
<p>Head Glabella Infraorbitale at Pupil Center Lt Ectoorbitale Lt Tragion Lt Back of Head Top of Head (Vertex)</p>		<p>Leg ASIS Lt and Rt PSIS Lt and Rt Lateral Femoral Epicondyle Lt Suprapatella Lt Infrapatella Lt Medial Femoral Epicondyle Lt Malleolus Lateral Lt Malleolus Medial Lt Heel Lt Ball of Foot Laterall Lt Toe (Longest Tibiale) Lt Ball of Foot Medial Lt</p>
<p>Leg Linkage ASIS Lt Lateral Femoral Epicondyle Lt Suprapatella Lt Malleolus Lateral Lt Toe (Longest Tibiale) Lt</p>		

3.6. Whole-Body Scanning

Body shape and surface contours were recorded using a Vitronic VITUS XXL full-body laser scanner and ScanWorX software by Human Solutions. The scanner, shown in Figure 5, uses red-light, eye-safe lasers mounted on four towers arranged in a square to project a horizontal line on the participant. Cameras mounted above and below the lasers in each tower record images of the laser line as the heads travel synchronously from top to bottom. Scanning the entire volume requires 12 seconds. The ScanWorX software converts the camera images to range data and then to 3D coordinate data. Approximately 500,000 surface data points are recorded with each scan. The system records grey-scale information for each data point, enabling visual identification of surface features. In some postures, body regions of interest that were shadowed from the whole-body scanner were measured using a hand-held infrared scanner.

3.6.1. Marking Landmarks

The locations of landmarks on the participants were recorded via skin targets stamped on the skin using the process shown in Figures 7-8. Body landmarks were marked on the skin using a pattern of water soluble, non-toxic, square ink stamp into which was placed a high contrast white paint dot. The combination was developed to provide good contrast on a wide range of skin tones that were chosen to produce targets that are readily viewed in the scan output. Small reflective hemisphere markers were taped to the shoulders of the child participants to track the location of the acromion landmark. Hemisphere markers also helped to prevent the safety harness from shadowing other torso landmarks. Figure 9 shows the locations of the stamped landmarks on a standing scan, and Table 4 gives a description of each marker. Appendix B presents marker definitions and locations.



Figure 7. Illustration of the process of palpating a landmark, placing markers on child participant's torso, stamping, and marking the contrasting centre.

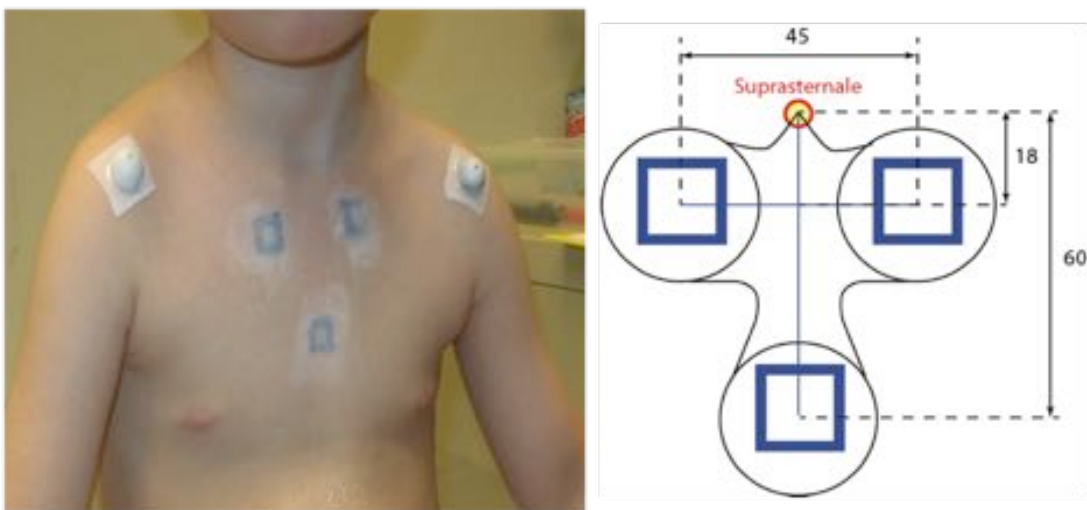


Figure 8. Torso landmark template.

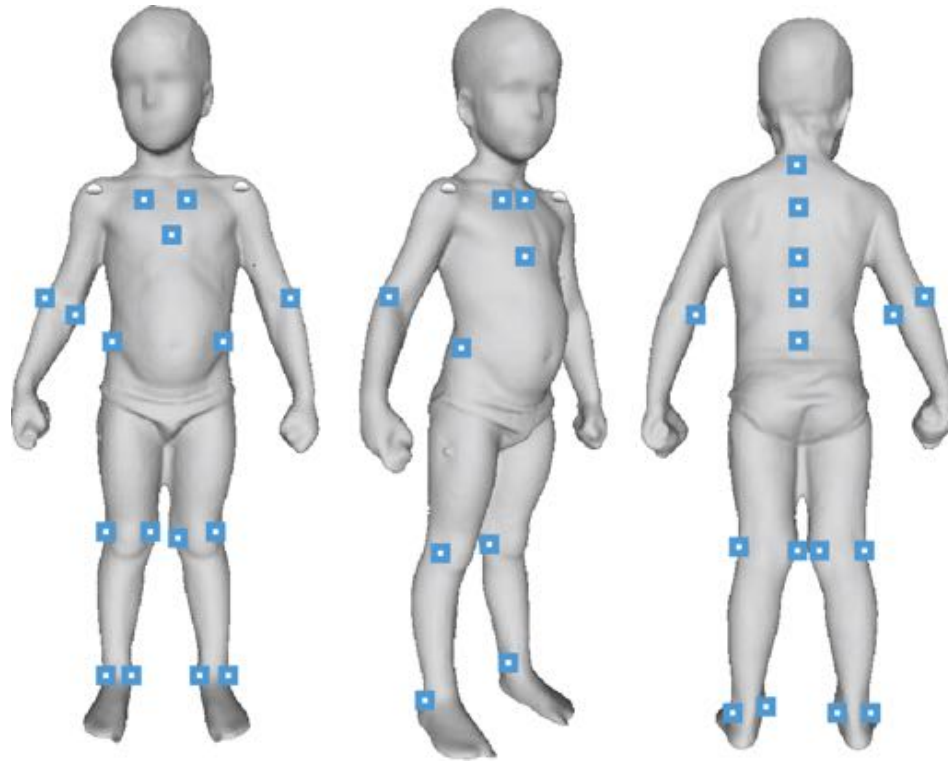


Figure 9. Position of Stamped Landmarks

Table 4. Landmarks Stamped on Skin Surface

Marker Name	Body Part	Description
AcromionLt_H	Torso	Hemisphere on anterior superior margin of acromion, Left
AcromionRt_H	Torso	Hemisphere on anterior superior margin of acromion, Right
ElbowMedLt_M	Arm	Medial epicondyle (marked with elbow bent 45°) (inside of elbow) , Left
ElbowMedRt_M	Arm	Medial humeral epicondyle (mark with elbow bent 45°), Right
ElbowLatLt_M	Arm	Lateral epicondyle (mark with elbow bent 45°) (outside of elbow) , Left
ElbowLatRt_M	Arm	Lateral humeral epicondyle (mark with elbow bent 45°), Right
SpineC07_M	Torso	Spinous process of the 7th cervical vertebra (cervicale)
SpineT04_M	Torso	Spinous process of 4th thoracic vertebra
SpineT08_M	Torso	Spinous process of 8th thoracic vertebra
SpineT12_M	Torso	Spinous process of 12th thoracic vertebra
SpineL03_M	Torso	Spinous process of 3rd lumbar vertebra
SternSup22Y18ZLt_M	Torso	Marker 18 mm down and 22 to left of suprasternale, Left
SternSub22Y18ZRt_M	Torso	Marker 18 mm down and 22 to right of suprasternale, Right
SternSup60ZCt_M	Torso	Marker 60 mm down from suprasternale
IlioLt_M	Torso	Marker on Iliocristale (most superior lateral point on pelvis) , Left
IlioRt_M	Torso	Marker on Iliocristale (most superior lateral point on pelvis) , Right
KneeFemMedLt_M	Leg	Femoral epicondyle, medial, Left
KneeFemMedRt_M	Leg	Femoral epicondyle, medial, Right
KneeFemLatLt_M	Leg	Femoral epicondyle, lateral, Left
KneeFemLatRt_M	Leg	Femoral epicondyle, lateral, Right
AnkleLatLt_M	Leg	Malleolus, lateral, Left
AnkleLatRt_M	Leg	Malleolus, lateral, Right
AnkleMedLt_M	Leg	Malleolus, medial, Left
AnkleMedRt_M	Leg	Malleolus, medial, Right

3.6.2. Scan Postures

Child participants were scanned in 17 postures listed in Table 5. The postures were chosen from among many considered to capture the range of body shapes expected in RF and FF CRS (Ebert et al., 2014). As well, postures were chosen to characterize the overall body shape in ways that could be compared to other datasets. Figures 10, 11, and 13-18 illustrate the scan postures.

Table 5. Scanning Postures

Posture	Code	Seat Pan	Seat Back	Hips	Lower Limbs	Spine	Shoulders	Hand Scan
Standing Abduction	T2	NA	NA		Knees apart	Natural	Abduction 40°	
Sitting Lap	L1	0°	NA	75°	Knees 90° Ankles under knee	Erect	Handles*	Yes
CRS-0	E0	0°	90°	Narrow Splay	Knee Obtuse	Erect	Flexion 0°	Yes
CRS-1	E1	0°	90°	Narrow Splay	Knee Obtuse	Erect	Handles*	Yes
CRS-2	E2	0°	90°	Wide Splay	Knee Obtuse	Erect	Handles*	Yes
CRS-3	E3	0°	90°	Wide Splay	Knee Acute	Erect	Handles*	Yes
CRS-4	E4	0°	90°	Narrow Splay	Knee Acute	Erect	Handles*	Yes
CRS-5	E5	0°	90°	Narrow Splay	Knee Acute	Erect	Flexion 0°	Yes
Sitting ISO	L2	0°	NA	90°		Erect	Flexion 90°	Yes
Spine Natural	V1	0°		75°	Legs and feet symmetrical with thighs parallel, ankles under the knees, and feet parallel	Natural	Handles*	
Spine Slouch	V1	0°		75°		Max Flexion	Handles*	
Spine Flexion Max	V2	0°		75°		Mid Flexion	Handles*	
Spine Flexion Mid	V3	0°		75°		Ext max	Handles*	
Spine Extension Max	V4	0°		75°		Erect	Flexion 90°	
Arm Flexion 90°	A1	0°		75°		Erect	Flexion 180°	
Arm Flexion Max	AY	0°		75°				

*Handles = Palm at height of suprasternale, shoulders as if arms were hanging at sides with elbows 45° out from body in coronal view and the shoulder-elbow-wrist angle at 120°

One standing posture (T2) and two unsupported sitting postures (L1, L2) were included to allow linkage to previous studies that would facilitate construction of ergonomic manikins. Figure 10 shows the standing posture that was a relaxed, symmetrical, natural standing posture, with feet 10 cm apart, and arms abducted 30° to improve laser coverage. Figure 11 illustrates the L1 unsupported sitting posture. In L1, the child participant sat with an erect and unsupported torso on a level seat in which the tops of the thighs are visible in the full body scanner. In an effort to standardize the upper extremity posture, investigators and caregivers assisted set the angle of arm relative to the midline of the torso in the transverse plane to 45° and position to an included elbow angle of approximately 120°. L2 was selected to be similar to the ISO standard anthropometric sitting posture with the arms vertical and forearms horizontal, forming a 90° included elbow angle.

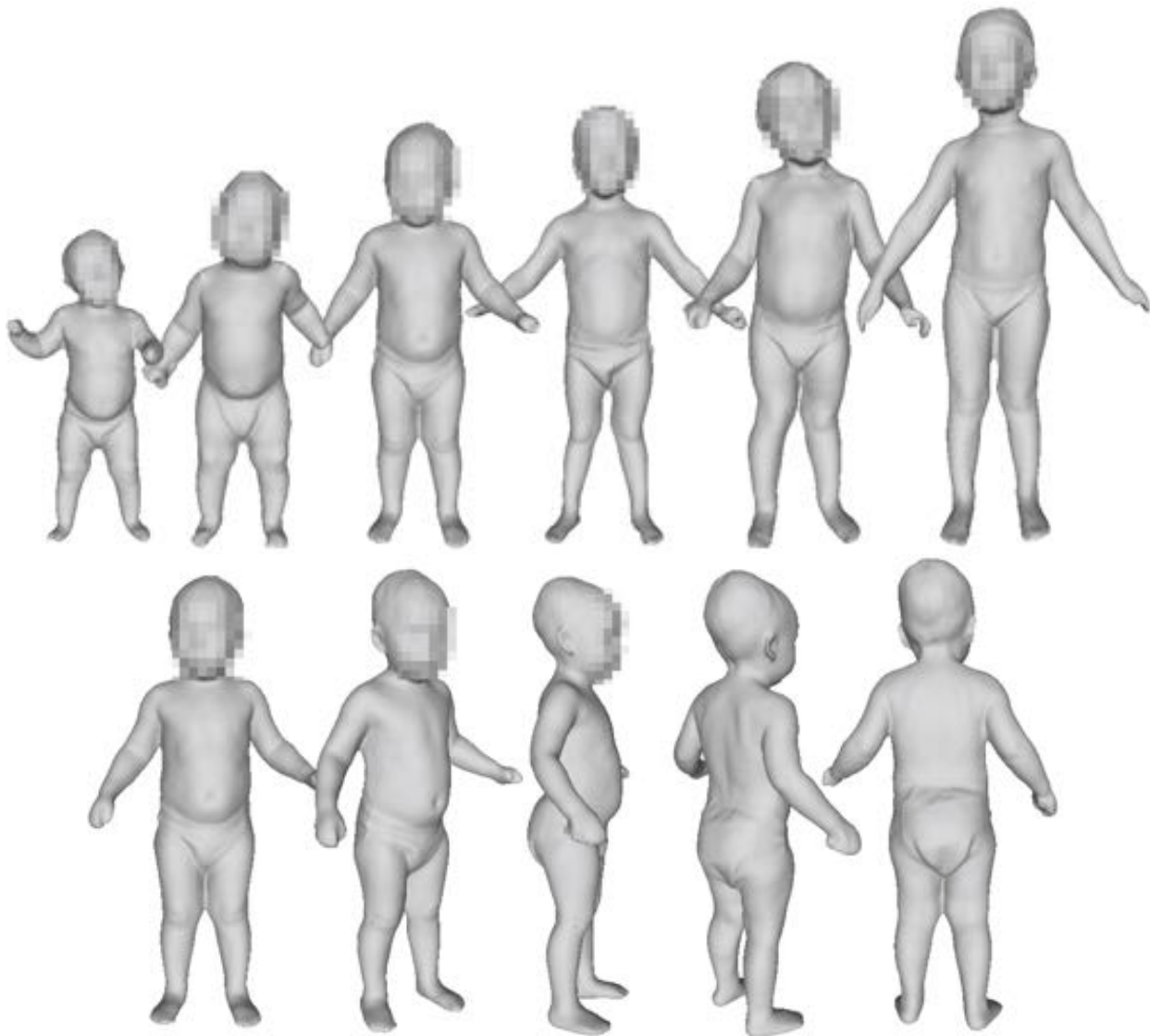


Figure 10. Standing posture (T2): natural with arms raised.

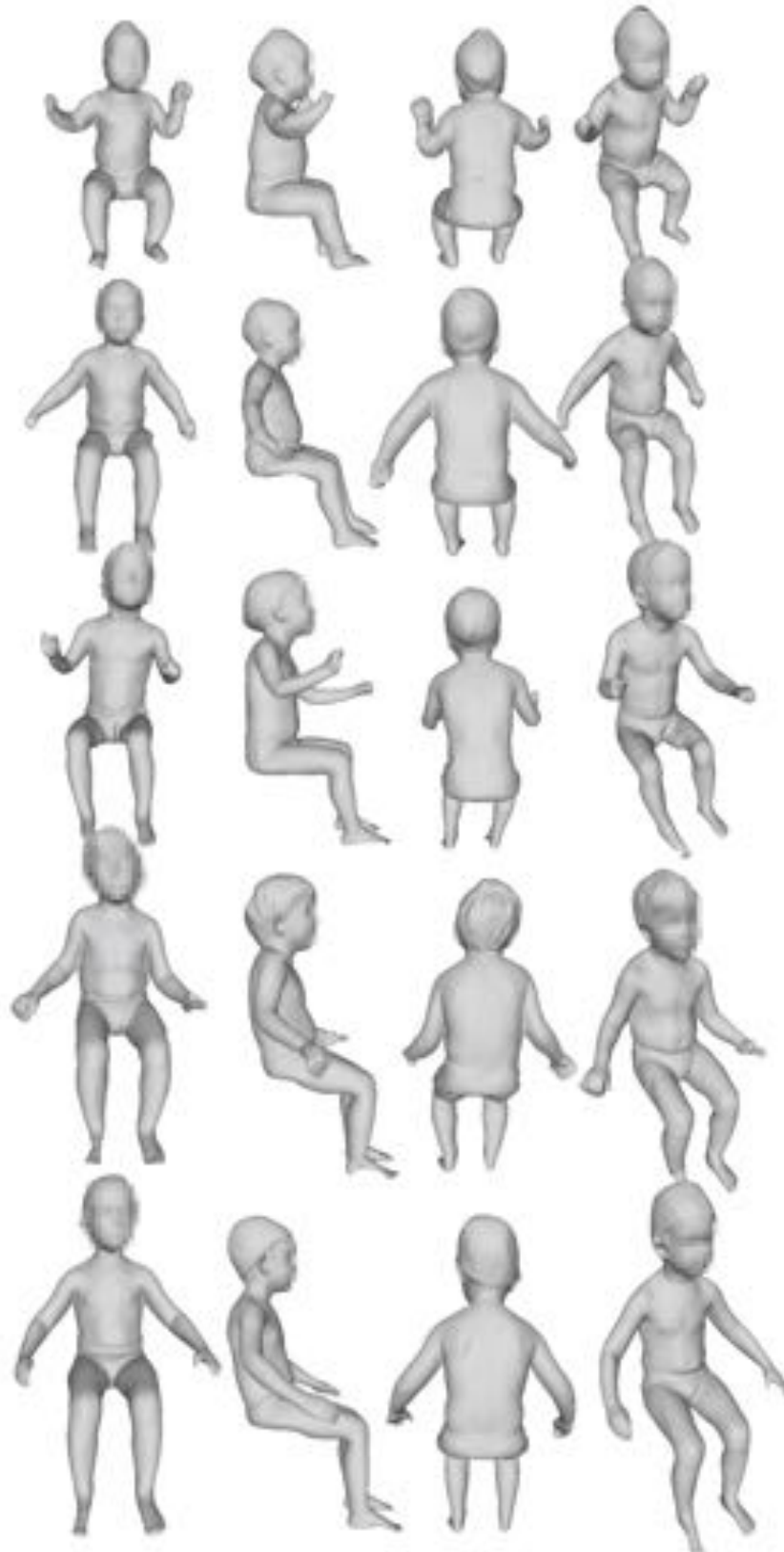


Figure 11. Unsupported sitting posture (L1).

The most important scans are the seven sagittally symmetric, supported CRS sitting postures (E0 through E5) as shown in Figures 13-16. These postures ranged through a series of lower extremity postures assumed by child participants in RF and FF CRS that were observed in the Ebert et al. (2014) study. The reconfigurable CRS seat fixture was set with a 90° seat back angle and a 0° cushion angle, and a reclined orientation for all of the supported CRS sitting postures. The lower extremity CRS postures were classified by a simplified hip splay angle and included knee angle. Hip angle was defined as the included flexion angle (Figure 12). Knee joint was defined as the included angle in the plane formed by the hip joint, knee joint, and ankle joint locations (Figure 12).

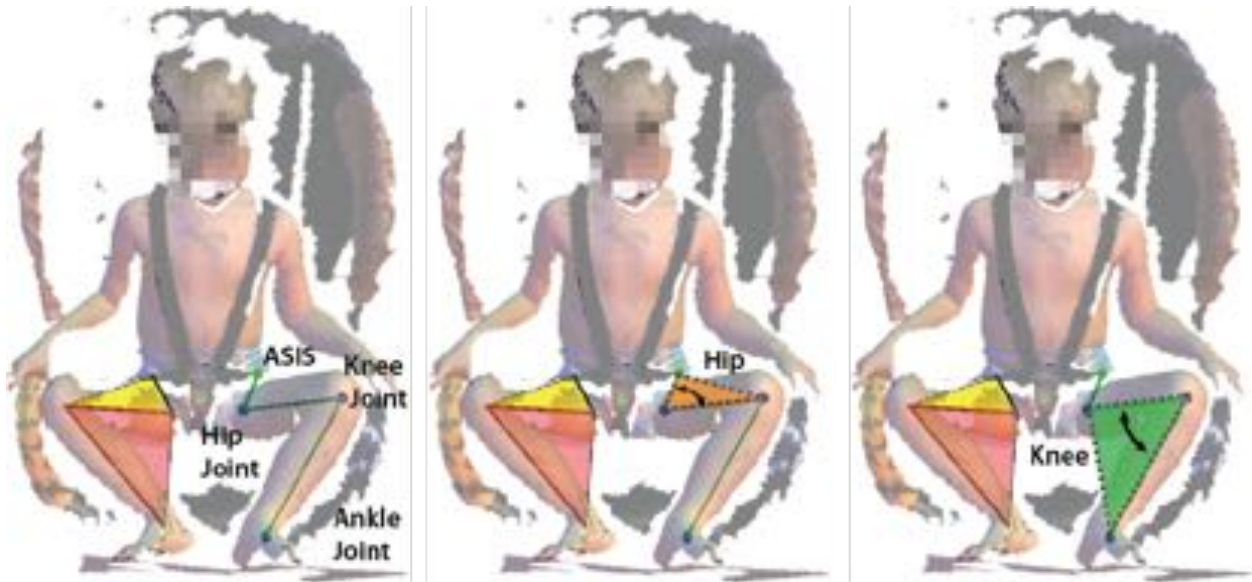


Figure 12. Plane defined by the ASIS, hip joint and knee joint. Included angles: 1) hip splay, and 2) knee angle.

In E0 and E1, child participants adopted a narrow hip splay angle and their feet were positioned to achieve an obtuse knee angle (Figure 13). Scan postures E5 and E4, were also defined by a narrow hip splay angle, while the feet were drawn in to achieve an acute knee angle (Figure 14). Each of the narrow hip splay postures were scanned twice: once with arms rested at the sides of the torso, while elbows and shoulder were relaxed with participants' hands were positioned on the handle to support weight of arms (E0, E5), and with the same arm posture as was used for the unsupported sitting posture to ensure that there was sufficient data collected on the torso contour (E1 and E4). In scan postures E2 (Figure 15) and E3 (Figure 16), child participants opened their hips to achieve a wide splay angle, positioned feet to accomplish an obtuse and acute included knee angle, respectively, both with the same arm posture as was used for the unsupported sitting posture.

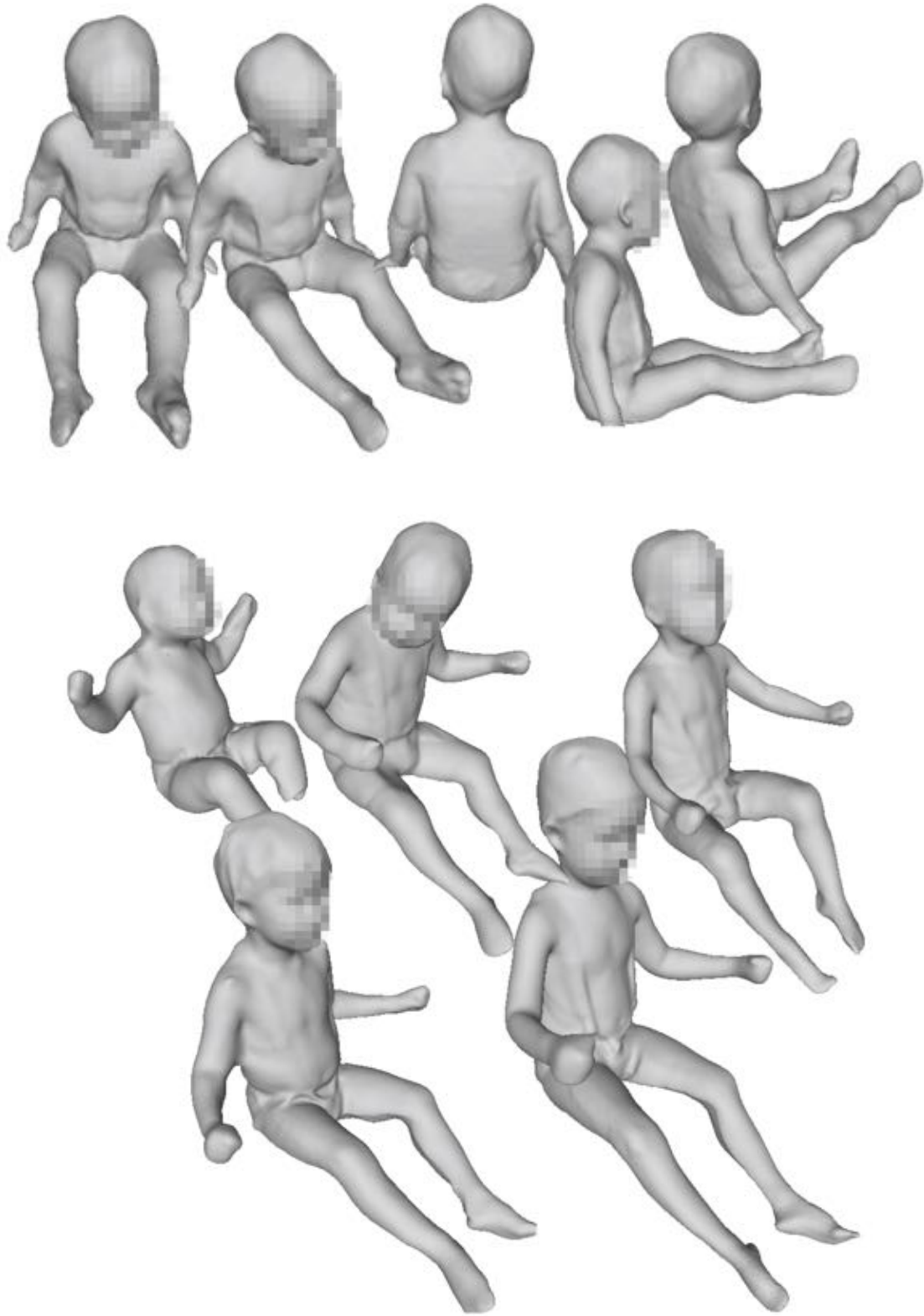


Figure 13. CRS posture with narrow hip splay and obtuse included knee angle (E0-top row, E1-bottom row)

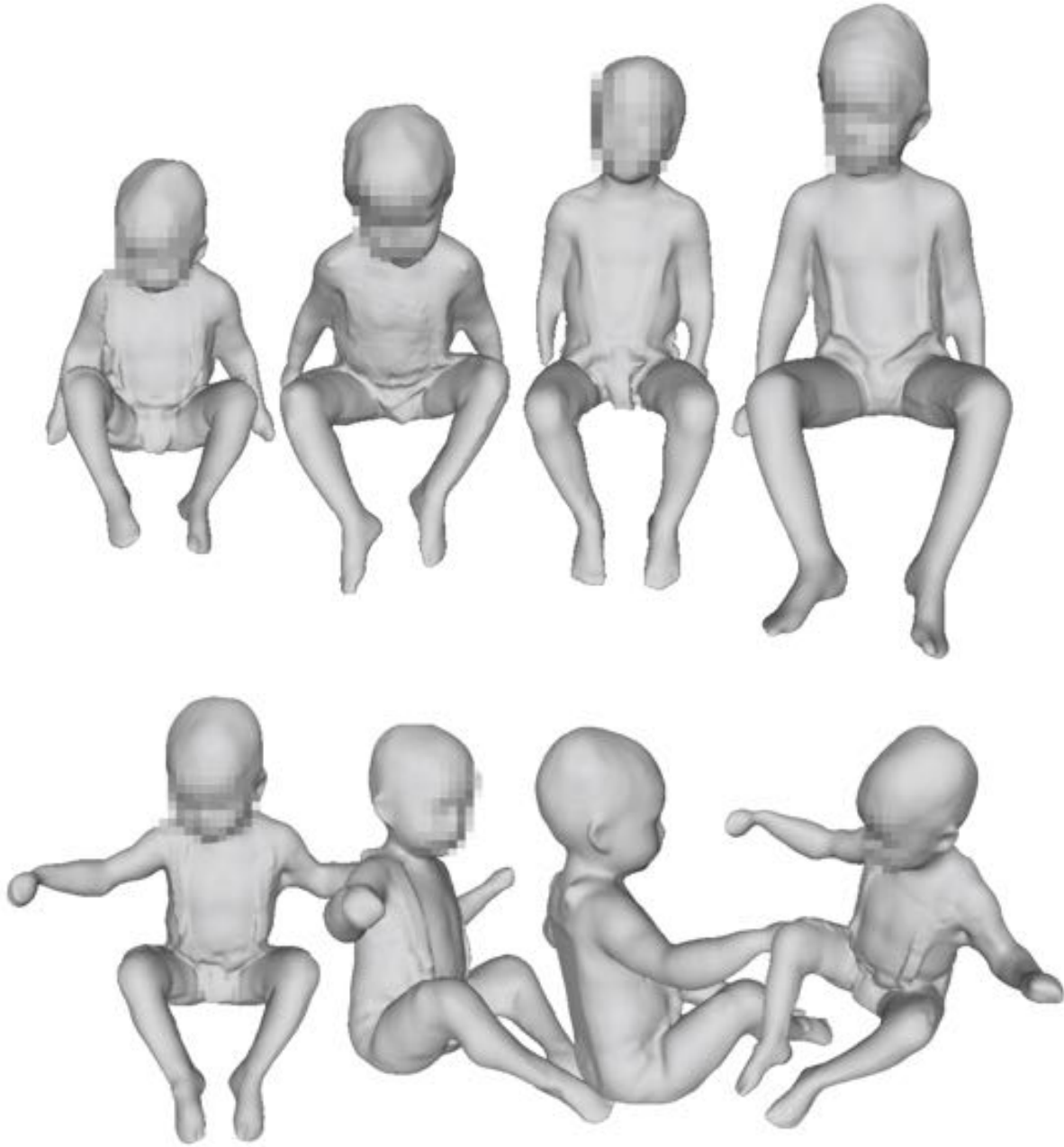


Figure 14. CRS posture with narrow hip splay and acute included knee angle (E5-top row, E4-bottom row)

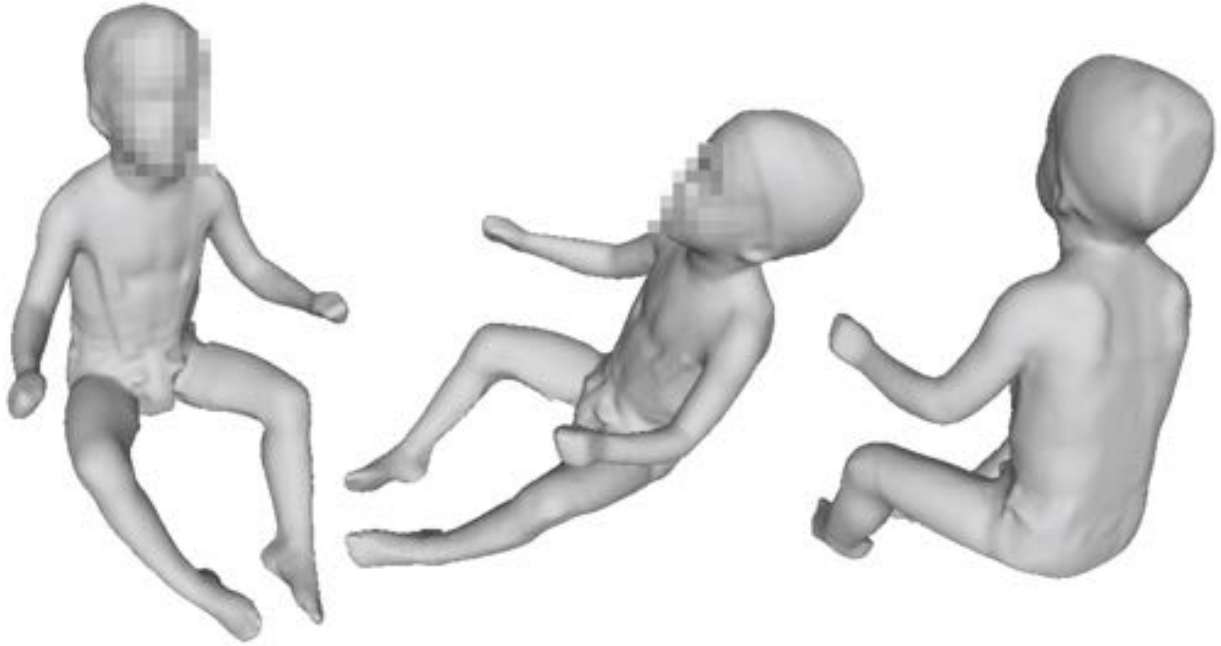


Figure 15. CRS posture with wide hip splay and obtuse included knee angle (E2)

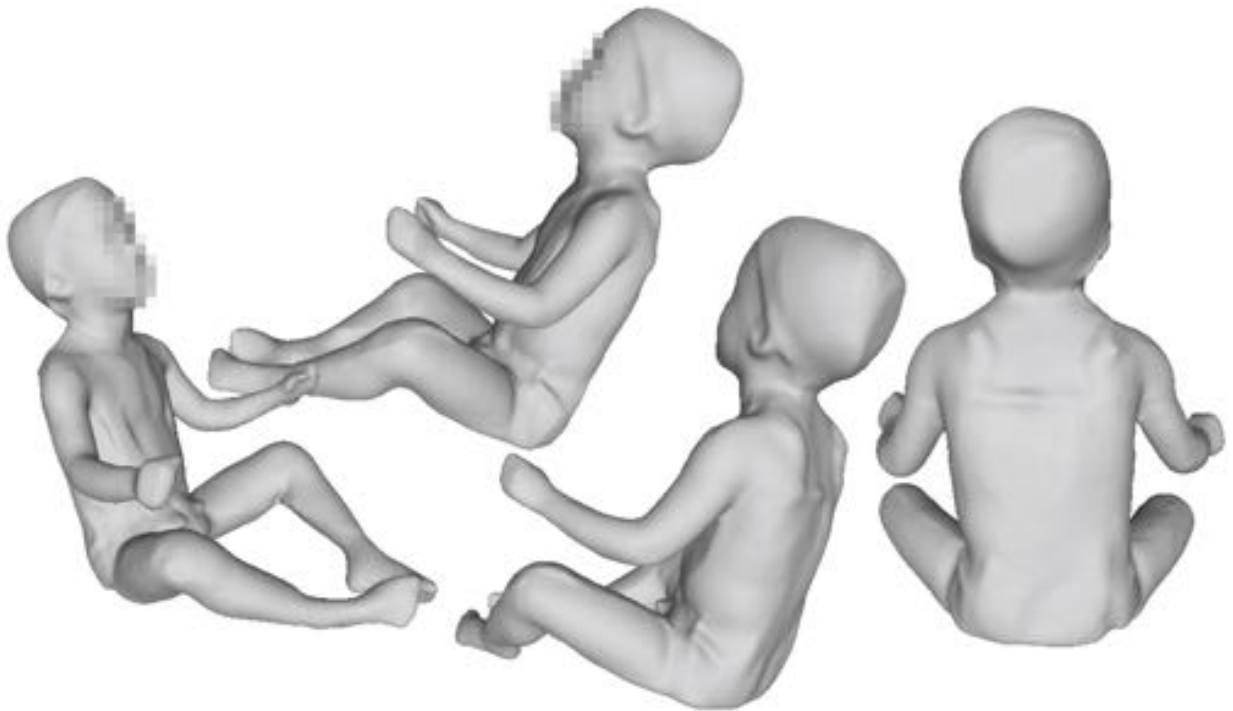


Figure 16. CRS posture with wide hip splay and acute included knee angle (E3)

Figure 17 shows a set of postures designed to document the torso shape across the lumbar spine range of motion, from three postures with unsupported torso (V1 through V3). Spine range of motion ranged from natural sitting position to maximal flexion in which child participants were instructed to rest their chin on their chest. Maximum extension (V4) involved extending the spine as far as could be safely accomplished. Scan postures A1 and AY involved two postures that demonstrate a range of shoulder flexion. Figure 18 illustrates surface geometry changes at the shoulder, neck and torso associated with upper-extremity posture. The primary goal of these postures was to quantify the changes in shoulder and torso shape associated with these motions, rather than to make accurate measurements of shoulder range of motion.

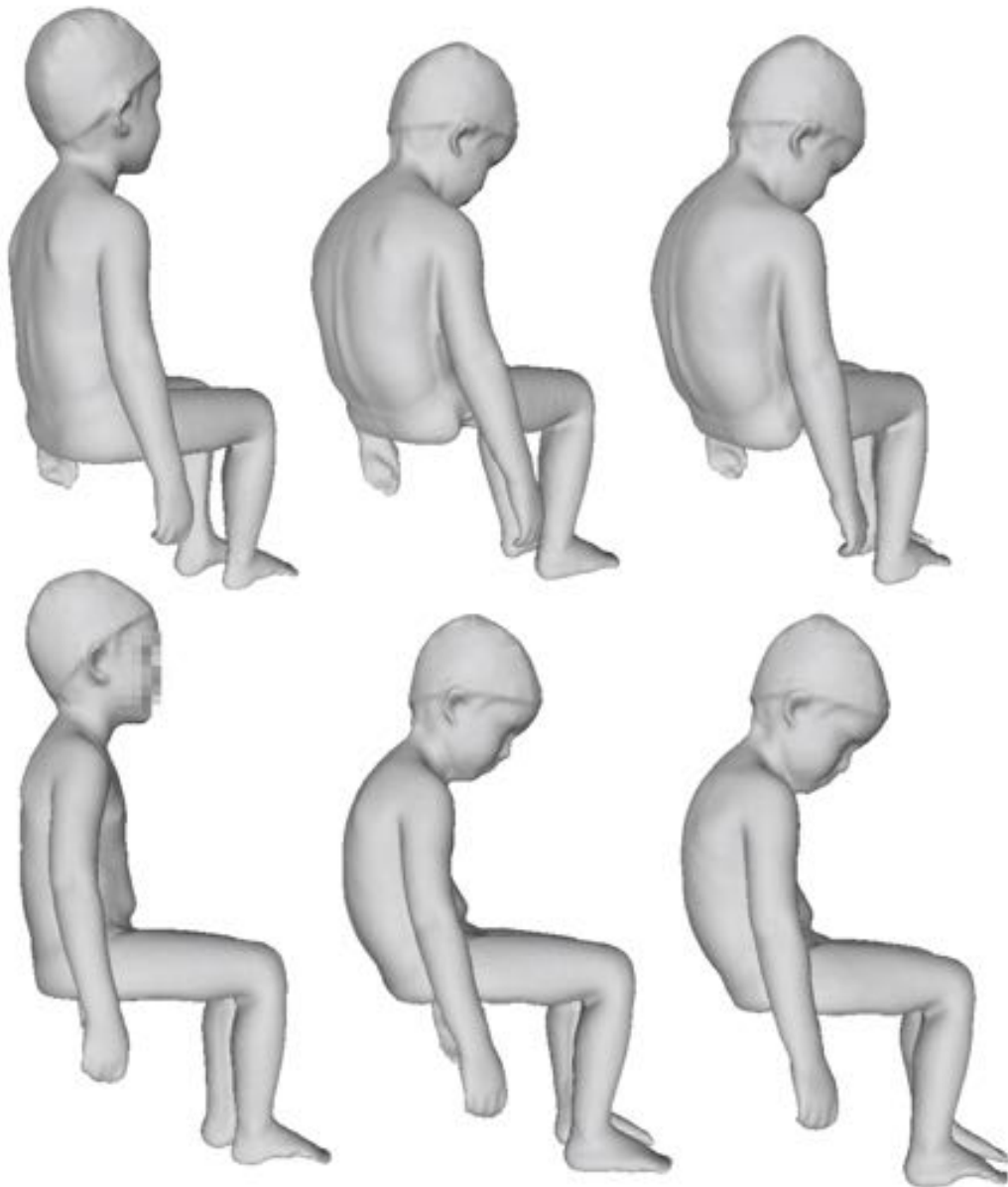


Figure 17. Spine range of motion postures (V1, V2, V3)

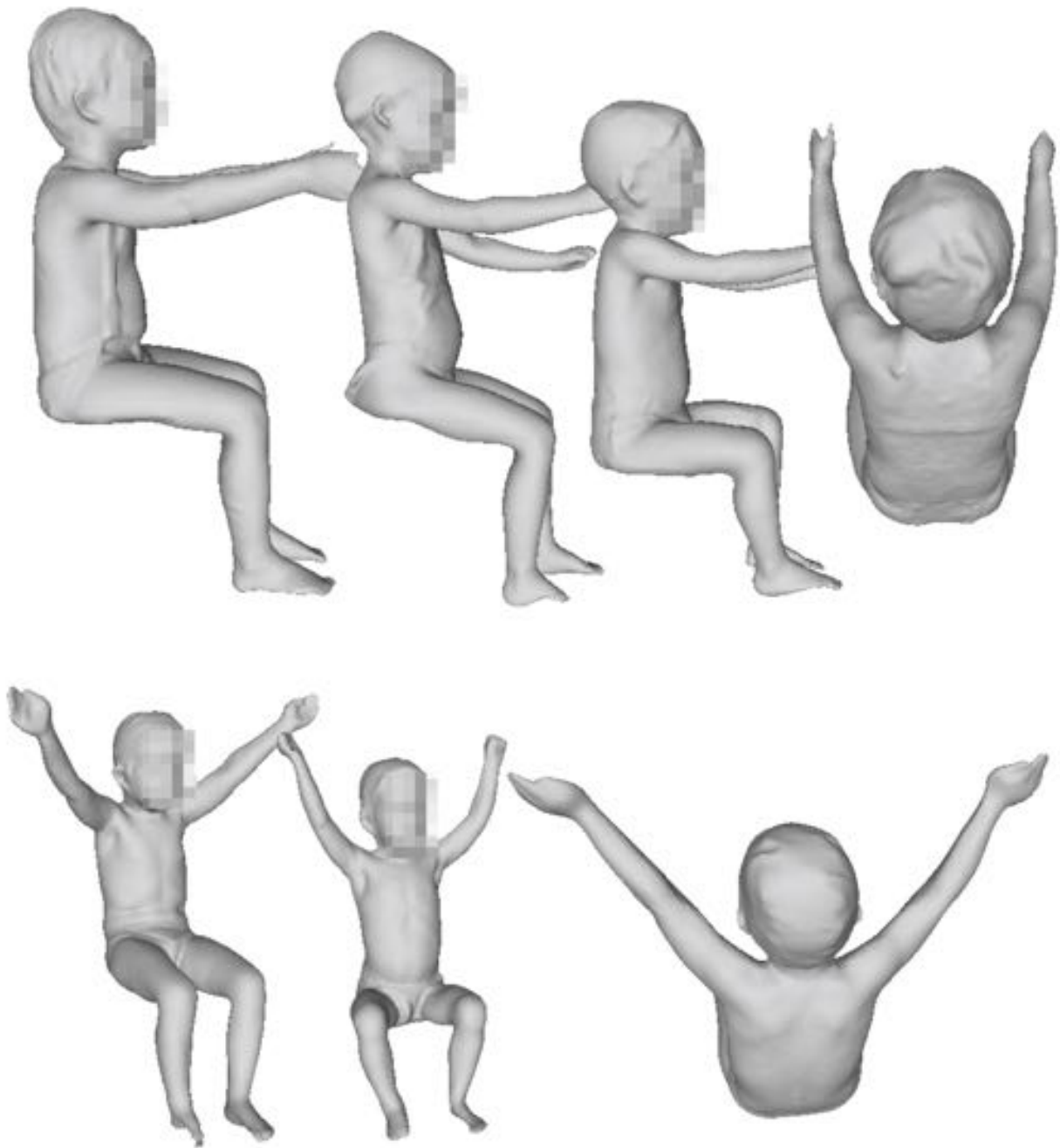


Figure 18. Shoulder range of motion postures
(A1-top row, AY-bottom row)

3.7. Protocol

The study protocol was approved by the University of Michigan Institutional Review Board (IRB) for Health Behavior and Health Sciences (IRB # HUM00091202). Participants were recruited through online advertisements and word of mouth. Written informed consent was obtained from the caregivers of each toddler participant. Due to the age of the child participants the protocol was designed to be modular to enable the researchers to have flexibility to change the sequence based upon the comfort, behavior or needs of the child participant. Extra care and time was spent introducing the toddlers and caregivers to the instruments and measurement protocols (i.e. standard anthropometry, reconfigurable CRS seat). The caregiver was also asked to assist and engage in all aspects of the protocol in an effort to put child participants at ease.

Child participants first changed into scan wear, consisting of a close-fitting swimsuit for those who were toilet trained; otherwise it was a pull-up style diaper and swim cap. Body landmarks were marked on the skin using a pattern of water-soluble, non-toxic body paint. Standard anthropometry was obtained from the toddler, followed by measurement in the hardseat, and scan postures in the reconfigurable CRS seat. A full-body scan was performed using the VITUS XXL system, and then the hand-held Sense infrared scanner was used to collect a duplicate set of contours focusing on the shoulders and pelvis area, where the whole-body scanner is more limited in its ability to collect good contours. Maintaining the child participant in a still posture for the duration of a whole-body scan was the greatest methodological challenge. Figure 5 illustrates participants seated in multiple postures, demonstrating how the postures were achieved using a combination of foot props, hand props, and caregiver guidance. Several measures were put in place to mitigate participant movement including: 1) the assistance of caregivers and researchers to stabilize a participant's posture, 2) customized fixtures to support the limbs, 3) use of props to distract children (for example, toys and electronic tablets), and 4) verifying and repeating scans during testing. Once the child achieved the targeted posture, the FARO arm was used to record the locations of key landmarks. All testing was completed in a single session lasting approximately two hours.

3.8. Scan Data Processing

Following data collection, an extensive processing and data extraction effort necessary to obtain high-quality scan and landmark data. The surface data obtained from the laser scanners were pre-processed in the ScanWorX software (Human Solutions, GmbH). First, the reconfigurable seat and artifacts (for example, handholds and foot-positioning aids) were removed manually. Multiple scans from the same posture were merged in Geomagic Studio software. Figure 19 outlines the processing steps required to obtain a complete composite surface of the 3D body shape. Data from the hand held Sense scanner is intended to augment the whole-body scan. Hand-held laser scans are used to record planar surfaces, such as the top of shoulders and thighs, and surfaces that interact with the harness restraint, which are shadowed from the primary scanner. The two scans are merged together to provide a more realistic composite 3D shape.

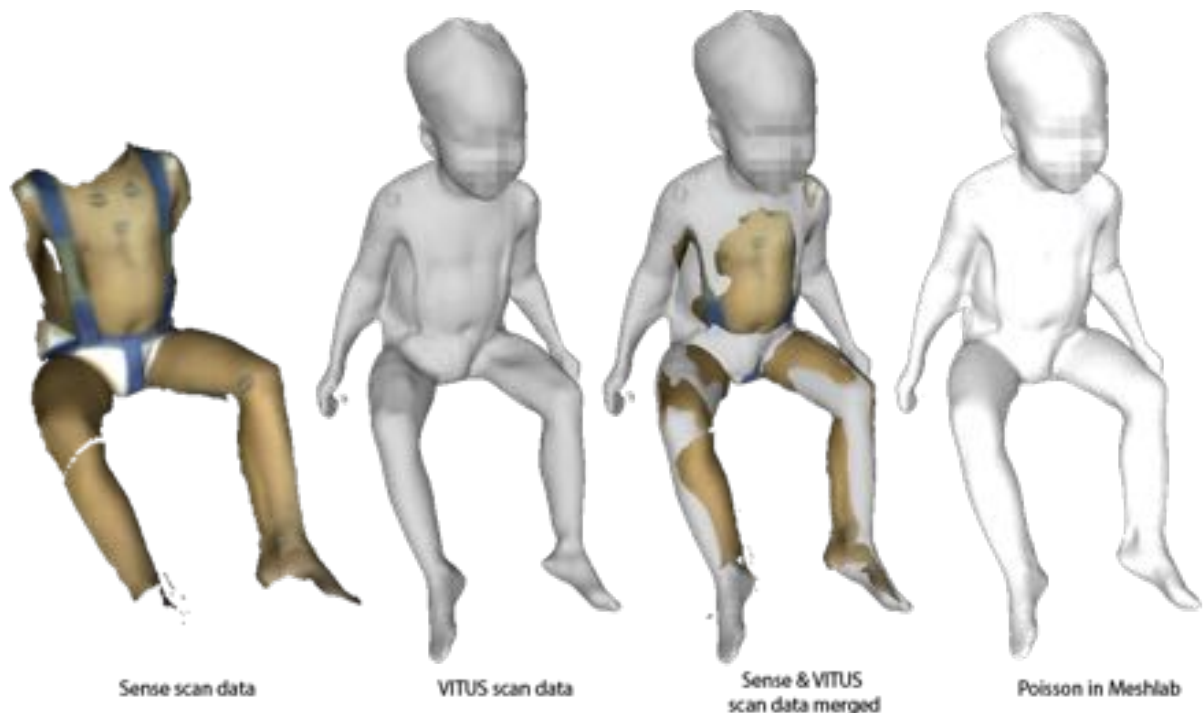


Figure 19. Processing steps. Handheld Sense scan data are merged with VITUS scan data to improve overall scan quality.

The next scan data processing step involved manually digitizing anatomical derived landmarks on the surface data. Research assistants used MeshLab software version 1.3.1 (meshlab.org) to extract landmark locations using a version of the scan data that included greyscale vertex coloring. Landmarks on the child participant define the position and orientation of the head, thorax, pelvis, upper extremities, and lower extremities. Some landmarks were also digitized on an “avatar” model generated in ScanWorX. The avatar has been processed to fill holes that can interfere with the digitizing process. Figure 20 shows the locations of the stamped landmark and digitized points on a standing scan. Figures 21-22 show screen shots of the landmarks extracted in MeshLab for representative scans. Appendix B provides complete detail on the marker definitions and digitized point locations.

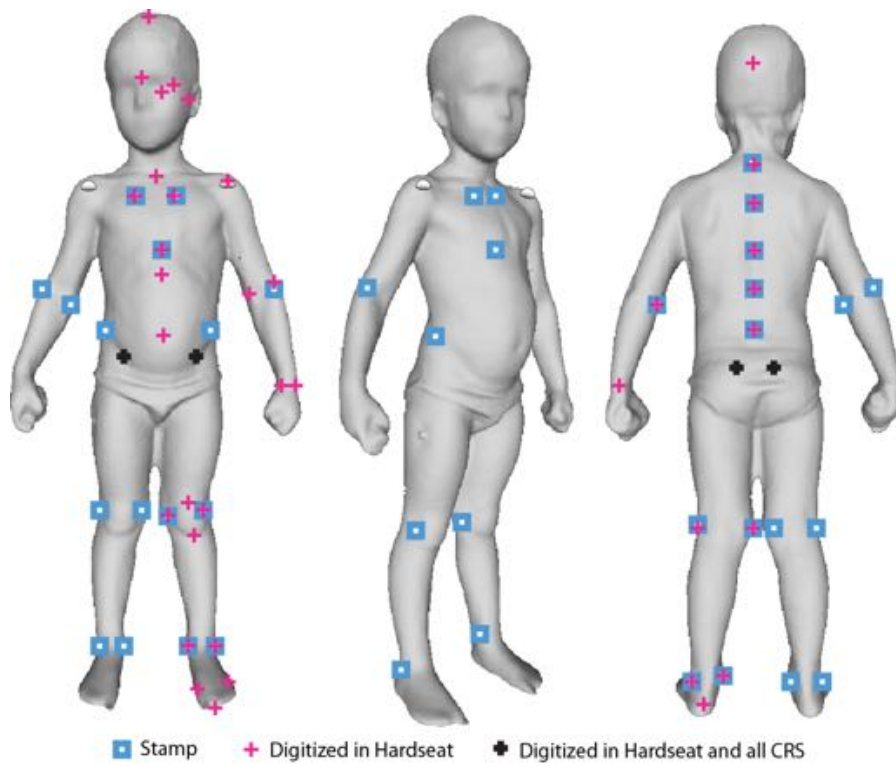


Figure 20. Stamps and digitized points.

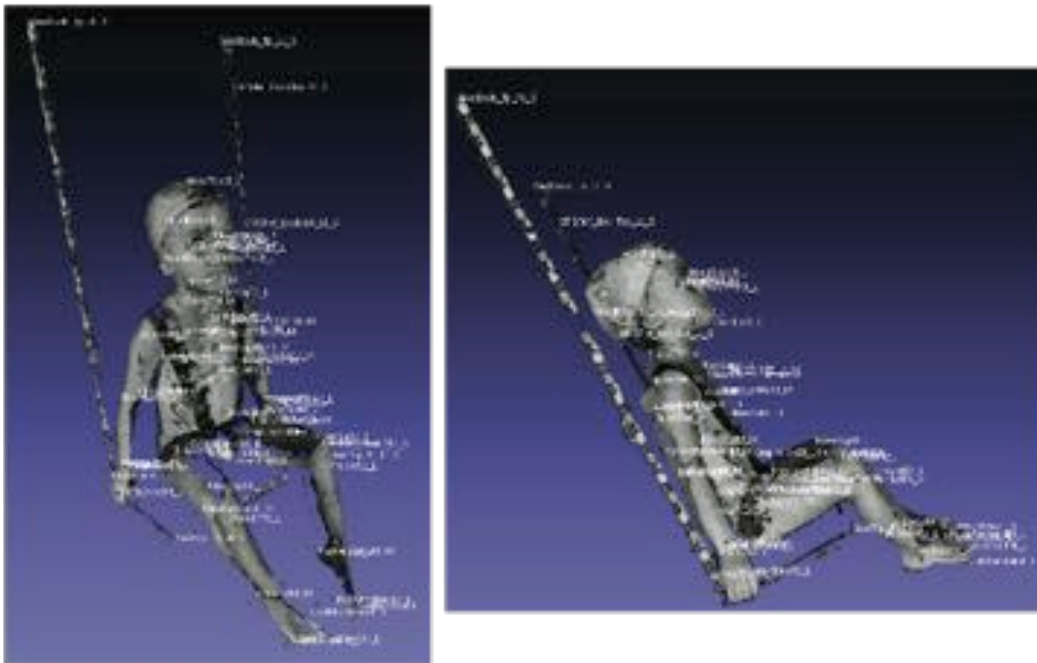


Figure 21. Examples of digitizing points and extracting landmarks in MeshLab from the seated CRS scan in greyscale mode.

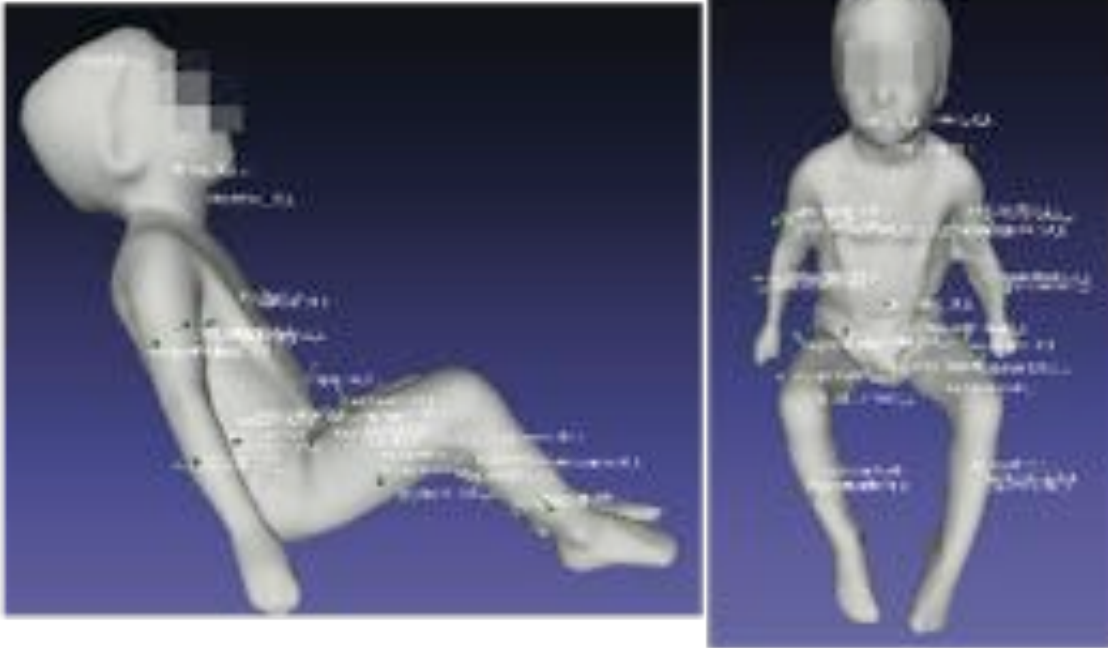


Figure 22 Examples of digitizing points on an avatar of a scan.

3.9. Body Shape Modeling

After landmark extraction, a statistical analysis on the combined landmark and body shape data was conducted using methods developed at UMTRI. To conduct statistical analyses of the scan data, it is necessary to express each scan using a consistent set of mesh vertices, such that each vertex is homologous across scans, meaning that it lies in the same location with respect to the anatomy. This was accomplished by fitting a template to each scan. However, the current project presented some exceptional challenges to the template fitting process as a result of significant postural variability for a given scan posture.

3.9.1. Toddler Scan Dataset

Some methodological challenges arose that were unique to the 1 to 4 year old toddler dataset, in comparison to adult and older children populations. The time duration of less than 12 seconds required for the whole-body laser scanner to capture the toddler's body shape proved too prolonged for some in the toddler aged participant pool. Several measures were put in place to minimize participant movement. Despite these efforts, significant postural variability resulted for a given scan posture. Figure 23 and 24 illustrate the posture variability in the unsupported sitting posture (L1), with most of the deviation observed in the upper extremity posture and head orientation. As a result, individual scan postures were not consistent across participants and new methods were needed to address the postural variability.

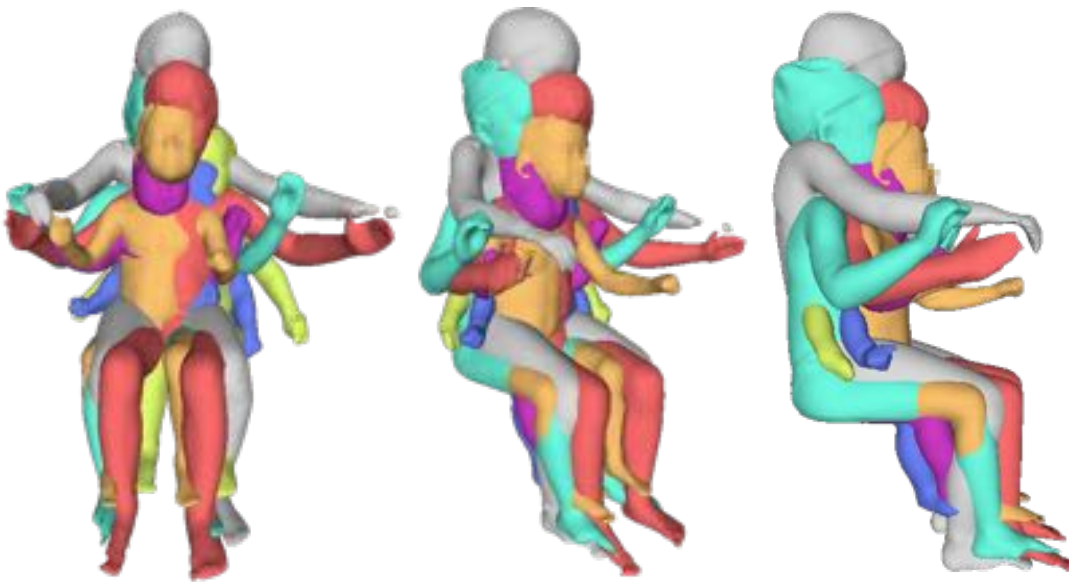


Figure 23. Overlay of participants in “same” unsupported sitting posture (L1). Child participants have substantial variability in arm position and head orientation.

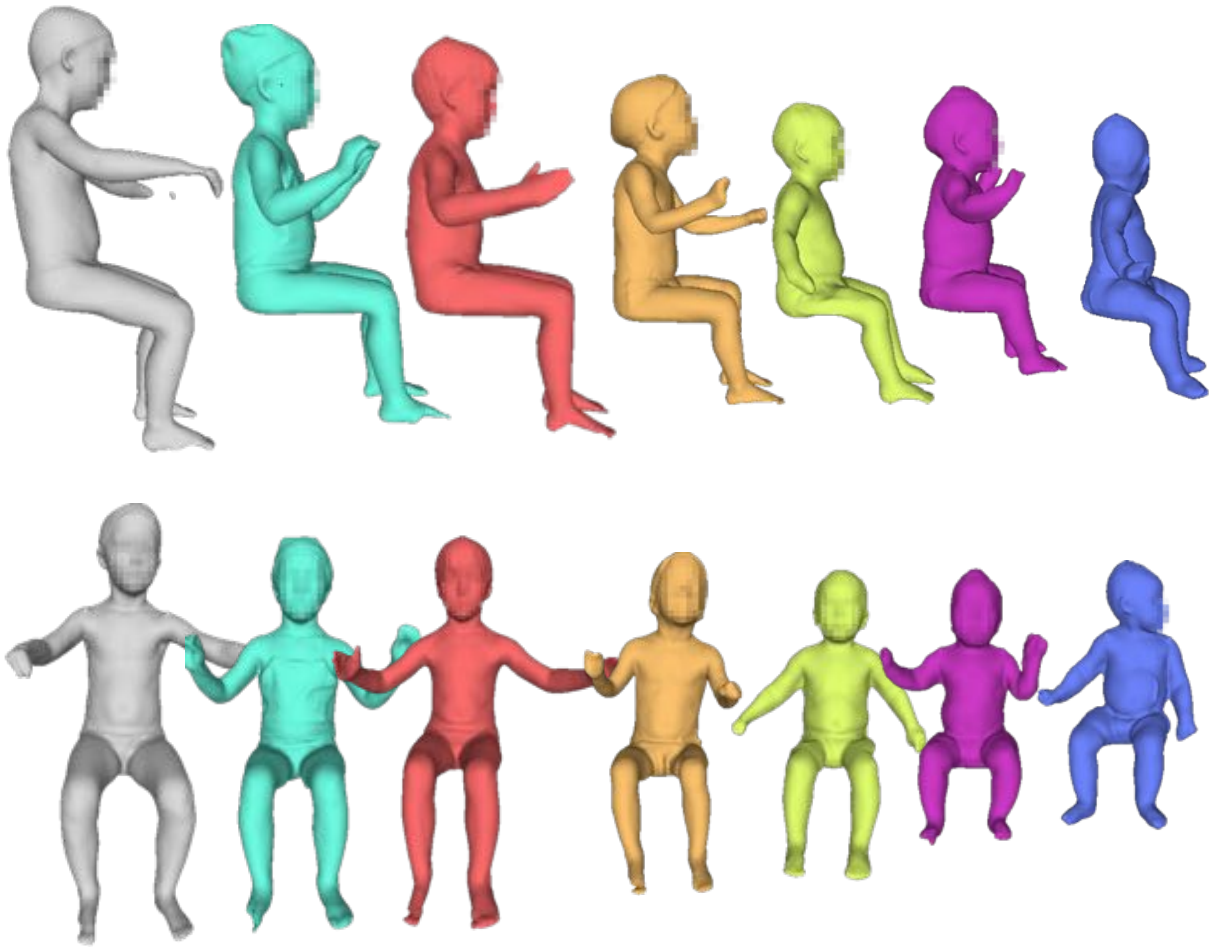


Figure 24. The participants exhibited considerable variation in body proportions and “pudginess.”

3.9.2. Reference Template

A reference template manikin was developed to homologically represent scan data. Open-source human modeling software MakeHuman v1.0.1 (www.MakeHuman.org) was used to make a template manikin. Figure 25 shows the reference template. The generated template was originally composed of 13,380 vertices. However, unnecessary geometry details, including the eyeballs, inner mouth, teeth, and inner ears, were removed. The final template consists of 11,449 vertices.



Figure 25. Reference template manikin generated from MakeHuman software.

The template geometry was imported and processed on 3-D data manipulation and visualization software Blender 2.71 (www.blender.org). On the template surface, landmarks were identified on the head/neck, torso, pelvis, upper and lower extremities. Table 6 outlines the template landmarks. Each landmark was attached to the nearest polygon of the template mesh using a local coordinate system defined by the nearest polygon vertices.

Table 6. Template Landmarks

Head/Neck		
HeadTop (Ct)	ChinTip (Ct)	EyeCor (Lt & Rt)
HeadBack (Ct)	Infrathyroid_ (Ct)	EyeCen (Lt & Rt)
HeadTrag (Lt & Rt)	NoseTip (Ct)	HeadGlab (Ct)
Gonion (Lt & Rt)		
Torso and Pelvis		
BustPoint (Lt & Rt)	SpineC07	Ilio (Lt & Rt)
SternSup22Y18Z (Lt & Rt)	SpineT04	CenterButtocks
SternSup60Z (Ct)	SpineT08	MidAbdomen (Lt & Rt)
SternSub (Ct)	SpineT12	CrotchMidThighHt (Ct)
Omphalion (Ct)	SpineL03	
Upper Extremities		
Acromion (Lt & Rt)	ArmUpperAnt (Lt & Rt)	ElbowLat (Lt & Rt)
AxillaFront (LT & Rt)	ArmUpperPos (Lt & Rt)	ElbowMed (Lt & Rt)
AxillaRear (LT & Rt)	ArmUpperLat (Lt & Rt)	WristLat (Lt & Rt)
	ArmLowerAnt (Lt & Rt)	WristMidBot (Lt & Rt)
	ArmLowerPos (Lt & Rt)	WristMed (Lt & Rt)
	ArmLowerLat (Lt & Rt)	WristMidTop (Lt & Rt)
Lower Extremities		
Hip (Lt & Rt)	LegUpperPos (Lt & Rt)	KneeInf (Lt & Rt)
ThighJnctLat (Lt & Rt)	LegUpperLatPos (Lt & Rt)	KneeSup (Lt & Rt)
ThighJnctMed (Lt & Rt)	LegUpperAnt (Lt & Rt)	KneeFemLat (Lt & Rt)
ThighJnctMidline (Lt & Rt)	LegLowerPos (Lt & Rt)	KneeFemMed (Lt & Rt)
InnerThigh (Ct)	LegLowerAnt (Lt & Rt)	AnkleMed (Lt & Rt)
	LegLowerLat (Lt & Rt)	AnkleLat (Lt & Rt)

3.9.3. Skeletal Linkage System for Template Posing

A skeletal link system consisting of 17 segments was developed and embedded into the template mesh (Figure 26). The linkage system was designed to articulate the template manikin to enable the template geometry to closely match with the scan data. Joint centers of the linkage segments did not coincide with anatomical joint centers. Torso, neck, and head joints are composed of 3-degree of freedom revolute joints. Elbow, knee, and upper-arm axial rotation joints have one degree of freedom rotation. Shoulders and hip joints are 6-degree of freedom “floating” joints, consisting of 3-degree of freedom rotation and translation.

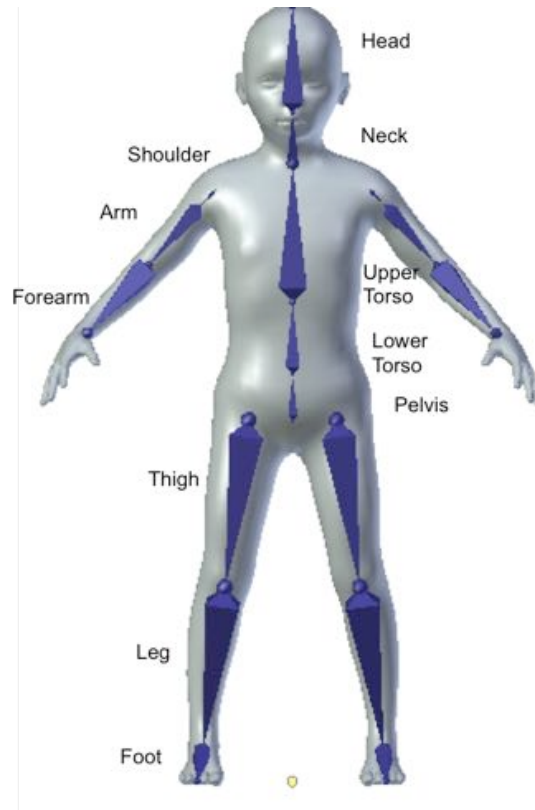


Figure 26. 17-segment link system for template articulation.

The scan geometry and landmarks was first translated and rotated to align the pelvis with the template manikin. Next, the overall template was scaled to match with the approximate size of the scan data. Template skeletal linkage was then articulated using both an automatic algorithm and manual adjustment. The automatic algorithm aligned the template landmarks with the scan landmarks, in an effort to minimize the sum of corresponding linear distances (errors) using a Procrustes analysis technique. Since the automatic algorithm alone in most cases did not entirely align the template to the scan data, the template was manually articulated and adjusted for fine details. Specifically, the orientation and scale of each segment was adjusted to match the surfaces of the template and scanned meshes (Figure 27). Whole body shapes of the template before and after the overall articulation process are illustrated in Figure 28.

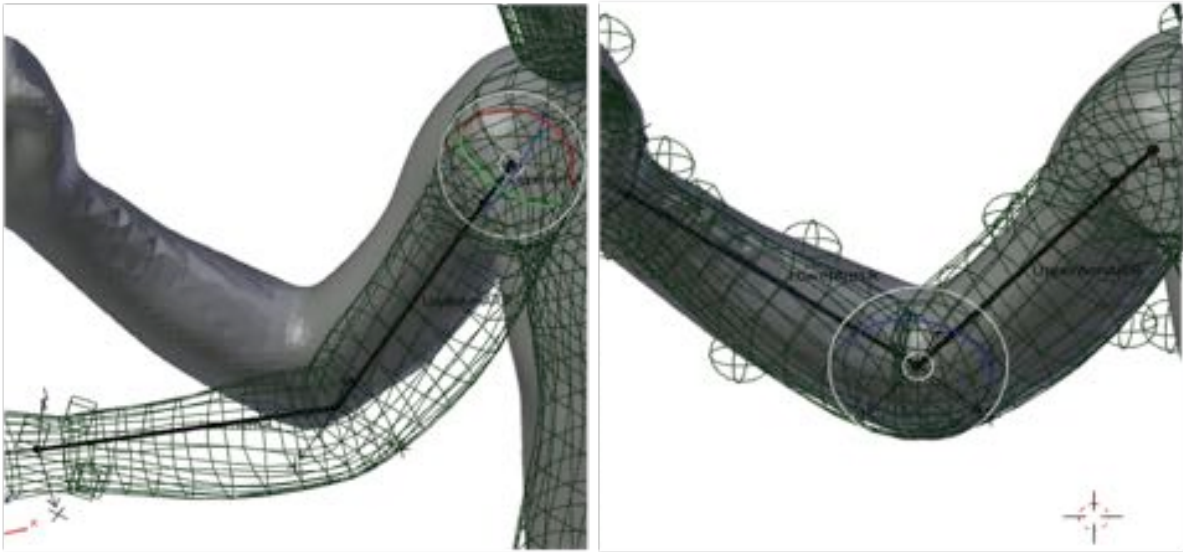


Figure 27. Before and after template articulation (wireframe manikin) to match the arm shape with the scan data (shaded manikin).

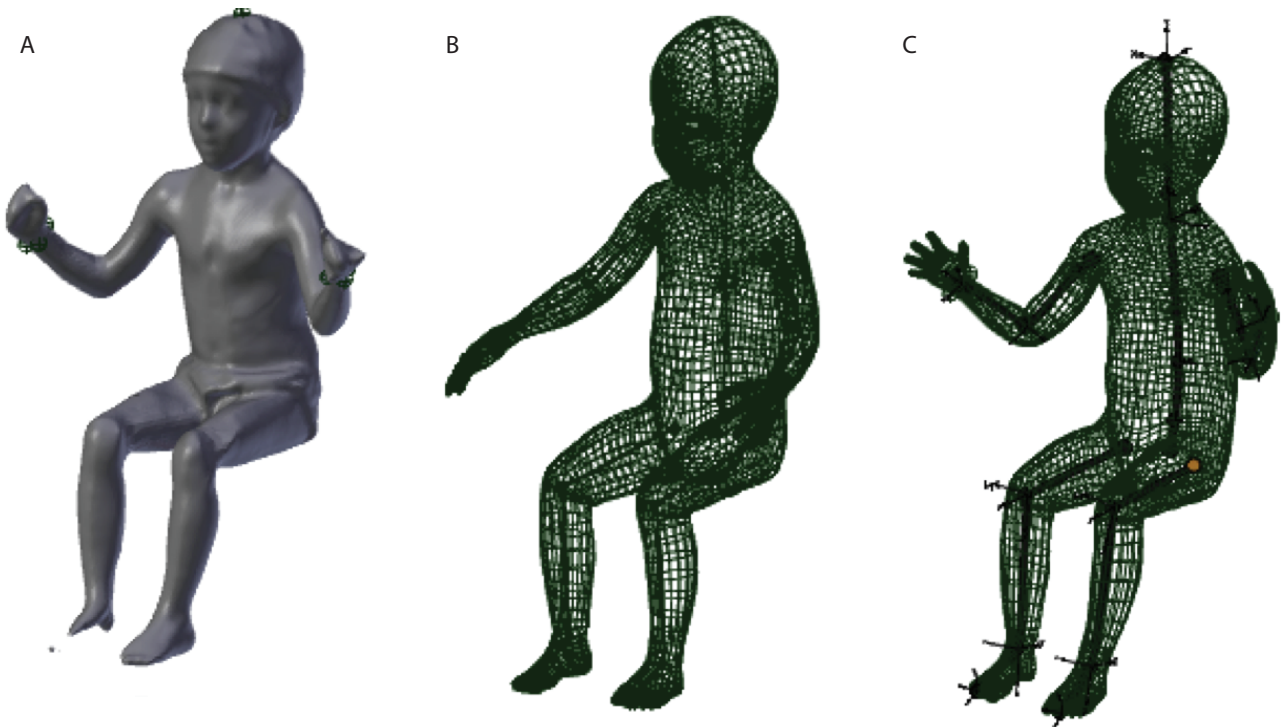


Figure 28. A: Scanned whole-body shape. B: Template before articulation. C: Template after articulation.

3.9.4. Morphing and Fitting

A non-rigid registration procedure (morphing) was applied to the articulated template. The morphing procedure was based on a radial-basis-function interpolation method (Park and Reed, 2015), which matched the landmark locations of the template and scanned mesh (coarse fitting).

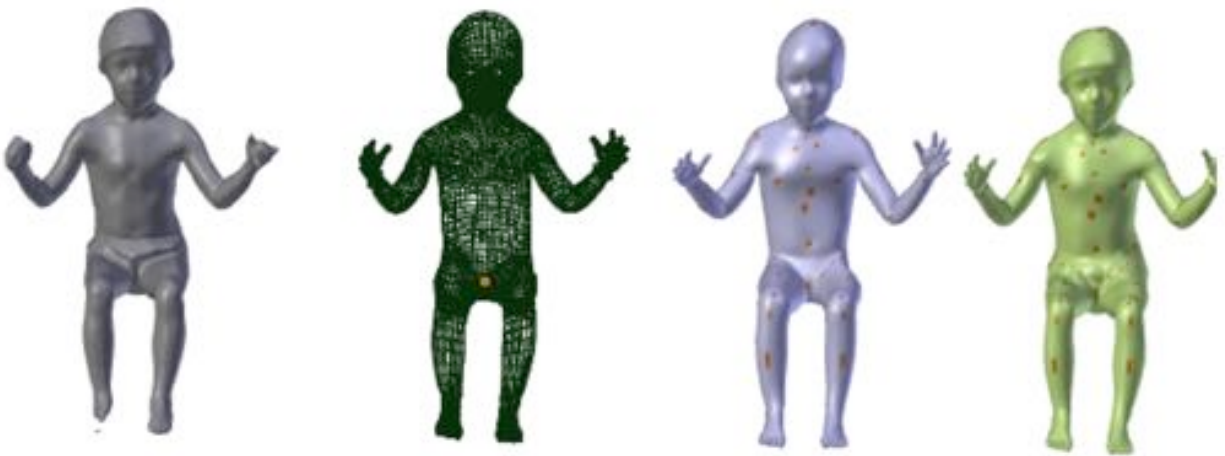


Figure 29. From left: scanned mesh, scaled template, articulated template, morphed template after implicit surface fit.

An implicit-surface fitting procedure reported in Park and Reed (2015) was used to move each vertex on the morphed template into correspondence with a mathematical surface defined by the scan data (fine fitting). The surface-fitting problem of the morphed template model was formulated using an implicit function constructed from the target scan data. The detailed steps of fine fitting process are summarized as follows:

1. Partition the target data into cuboids each of which contains approximately 400 vertices using a $k-d$ tree method.
2. Within each partitioned group of vertices:
 - a. Assign each surface point a scalar value of zero.
 - b. For a subset of the surface points, construct new points that are “inside” and “outside” the surface. Inside and outside points are created by moving along the normal by a margin.
 - c. Assign each inside point a value of -1, each outside point a value of 1.
 - d. Compute an interpolation function (Input: 3-d coordinates, output: 1-d scalar) using a radial basis function, of which value was assigned to zero on the surface.
3. Move each vertex on the template onto the surface (zero-valued position) using the gradient in the implicit surface function.

3.9.5. Posture Standardization

Due to the large variability of child participants' postures in scanned body shapes, the posture of the fitted manikin was reposed to match with a "standard" posture by articulating the skeletal link system embedded in the fitted manikin. The standard posture was obtained by taking an average of joint angles of all participants (Figure 30). Specifically, a quaternion representation of joint angles was recorded for each participant to calculate a mean quaternion (Horn, 1987, Humbert, Gey et al., 1996).

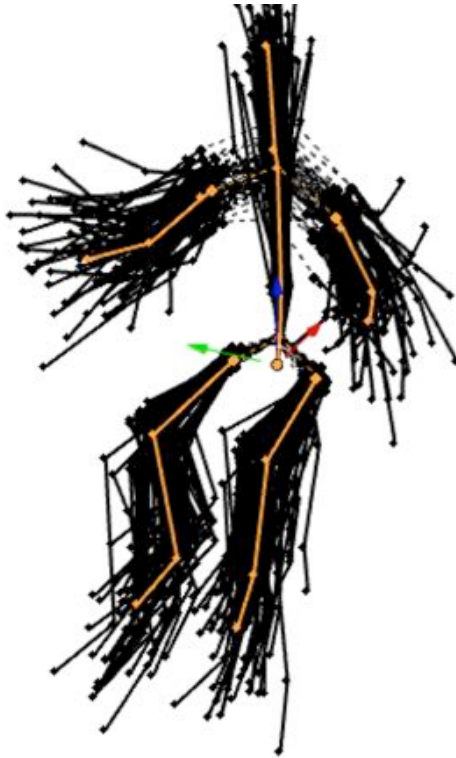


Figure 30. Posture variability across the participants (dark stick figures) and a standard posture estimated from mean joint angles (highlighted stick figure).

Each of the fitted scans was articulated to align the skeleton with the standard posture ("reposing"). During the reposing process, only the joint angles were manipulated and the segment lengths were not modified. Figure 31 illustrates fitted manikins before and after reposing. The reposed manikin was translated so the origin of the coordinate system coincides with the center buttock landmark position. The vertex and landmark coordinates of the reposed manikin was then exported and stored for the subsequent bootstrapping process (described below).

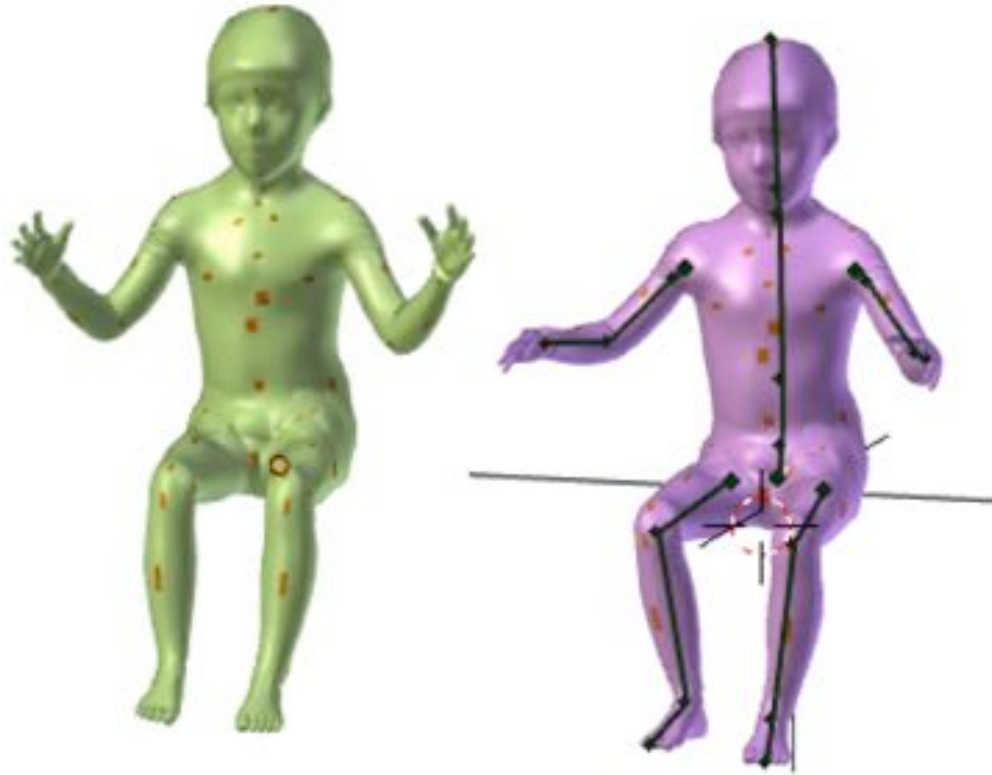


Figure 31. Manikins before (left) and after (right) reposing to the reference posture (stick figure).

3.9.6. *Bootstrapping for Participant-Specific Template Generation*

Since the body shapes tend to significantly vary with the participant's age, anthropometry and other factors, the shape of the reference template manikin, generated from MakeHuman software as described above, may be significantly different from the scanned body. In such cases, the fitting process may not yield accurate representation of the body shape due to the large initial errors between the template and the scanned body.

A bootstrapping process was used to generate participant-specific template manikins. Fitted, reposed surface meshes from a subset of participants were used to develop a statistical body shape model (SBSM) using the methods described below. The SBSM was used to create a target template for each participant using body mass index (BMI) and sitting height as predictors.

The new participant-specific template significantly improved the initial fit with the scanned body shape (Figure 32). The fitting and reposing processes described above were repeated using the bootstrapped template manikins. Bootstrap templates substantially improved the accuracy and efficiency of fitting and reposing processes overall. The final outcomes (vertex and landmark coordinates of the fitted/reposed manikins) were exported for further statistical modeling.



Figure 32. Scanned body shape (A). Template manikins originally generated from the MakeHuman software (B) and template generated using bootstrap technique (C).

4. RESULTS

4.1. Participants

Forty-seven child participants (30 girls and 17 boys), ages 1 to 4, were recruited in three categories of body mass index (BMI): less than 16.5 kg/m², between 16.5 and 17.5 kg/m² and >17.5 kg/m², and six categories of stature that ranged from 60 to 120 cm, in 10 cm increments. Standard anthropometric measures were taken on each participant to characterize overall body size and shape using manual measurements described in Appendix A. All measurements were obtained with the participants minimally clad. Table 7 summarizes the standard anthropometric data.

Standard anthropometric were taken in multiple postures (standing, seated, and supine) when possible to provide preliminary data on how these anthropometric measures vary with posture. Appendix C presents the results of the evaluation of the agreement between the standard anthropometric dimensions recorded in different postures.

Table 7. Standard Anthropometry: Selected Dimensions for the participant pool of 47 toddlers.

Dimension	Female			Male		
	Min	Mean	Max	Min	Mean	Max
Age (months)	11.9	31.8	58.2	13.8	34.2	58.6
Weight (kg)	9.1	12.7	19.4	9.3	15.2	23.2
Stature	725.0	904.9	1239.0	744.0	966.1	1197
BMI (kg/m ²)	13.8	16.1	19.5	14.1	17.0	20.7
Erect Sitting Height	442.0	521.1	606.0	450.0	551.8	680.0
Seated Eye Height	357.0	423.8	512.0	370.0	448.6	554.0
Acromial Height	268.0	316.3	376.0	278.0	332.5	404.0
Knee Height	195.0	254.7	312.0	206.0	277.5	340.0
Shoulder-Elbow Length	133.0	176.1	215.0	157.0	203.1	239.0
Elbow-Hand Length	200.0	241.2	264.0	213.0	271.3	308.0
Buttock Knee Length	196.0	271.0	348.0	207.0	299.9	366.0
Buttock-Popliteal Length	177.0	231.8	298.0	138.0	243.6	307.0
Chest Depth (Spine)	103	115.5	134.0	105.0	124.6	143.0
Bispinous Breadth	106	121.9	144.0	107	128.4	157.0
Biacromial Breadth	167.0	185.8	207.0	169.0	197.0	226.0
Shoulder Breadth	198.0	236.5	282.0	225.0	256.8	279.0
Maximum Hip Breadth	115.0	180.2	224.0	142.0	196.5	243.0
Tragion to Top of Head	80.0	103.3	115.0	101.0	117.4	221.0
Head Length	141.0	164.9	181.0	153.0	169.4	193.0
Head Breadth	122.0	132.5	149.0	124.0	135.4	147.0
Chest Circumference (Axilla)	446.0	499.9	609.0	470.0	531.5	578.0
Waist Circumference	446.0	491.9	576.0	289.0	501.0	580.0
Hip Circumference (Buttocks)	431.0	510.1	595.0	465.0	538.6	620.0
Upper Thigh Circumference	236.0	294.3	343.0	238.0	310.9	383.0

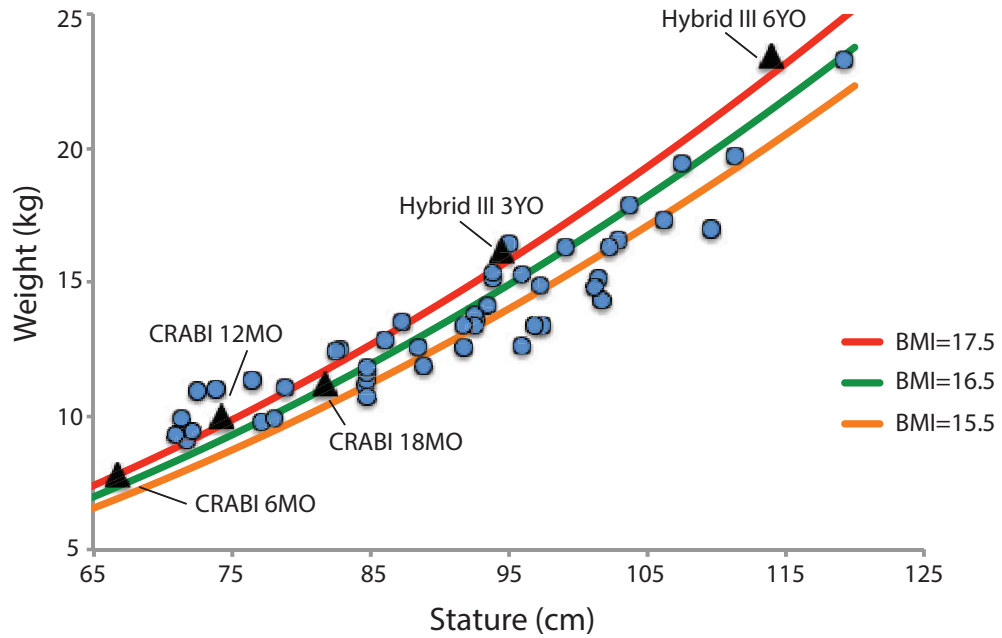


Figure 33. Weight (kg) versus stature (cm) for the child participants. Lines of constant body mass index (BMI) are overlaid. Distribution of the current child ATD overlaid (black triangles).

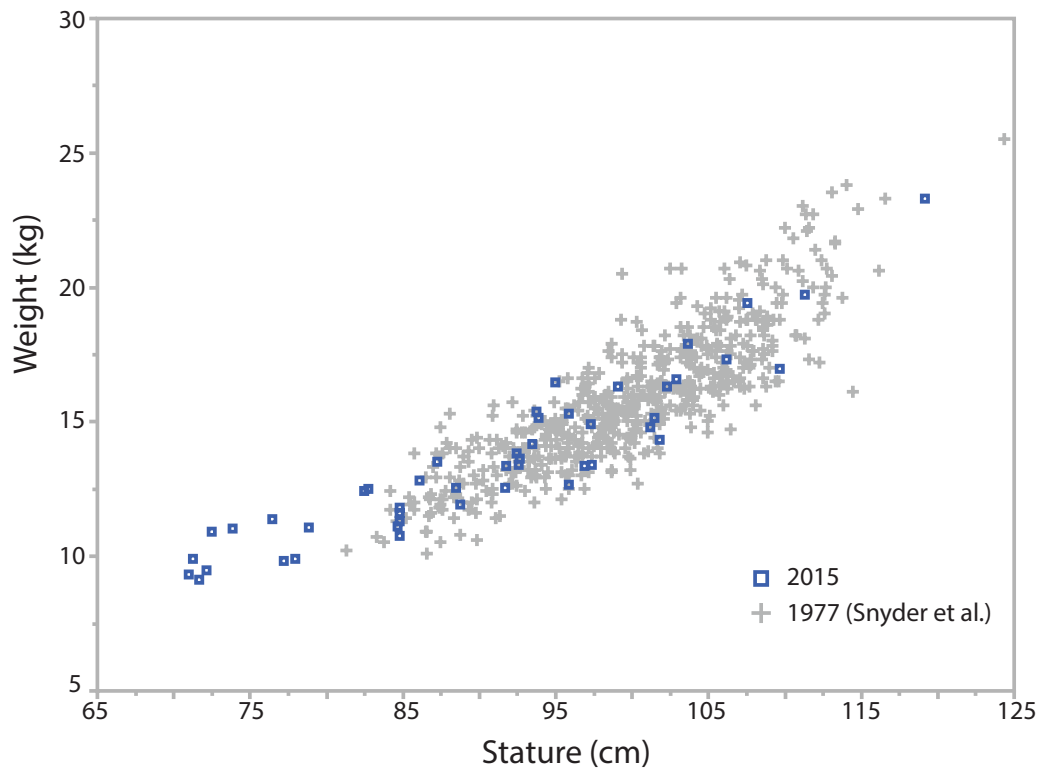


Figure 34. Distribution of the current child participants relative to the Snyder et al. (1977).

4.2. Body Shape Data

A total of 487 whole-body scans were gathered and processed in this study. Tables 9-12 illustrate some of the scans recorded and the range of postures. Appendix B lists the landmarks digitized on each scan. Tables 8 list the number of scans successfully gathered in each conditions. Table 8 includes counts from Ebert et al. (2014).

Table 8. Overall Count per Scan Posture

Posture	Scan Count	Posture	Scan Count
VT2	73 (42/31)*	VL2	12
VL1	72 (41/31)*	VLS	5
VE0	44	VA1	16
VE1	33	VAY	15
VE2	29	VC1	4
VE3	33	VV1	4
VE4	26	VV2	26
VE5	24	VV3	9
VE6	7	VV4	13

*current/Ebert et al. (2014) study

Table 9. Counts for Standing and Unsupported sitting postures

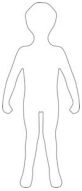

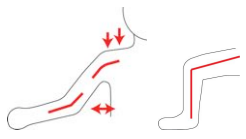

Posture	Description	Partial Illustration	Example	Count
T2 Standing Abduction	Feet apart on lines, knees apart Arms abducted 40°			73 Total Current study 42 Previous study 31
L1 Sitting Lap	No splay, thigh angled down, ankle under knee, chin up Arms away from body			72 Total Current study 41 Previous study 31

Table 10. Counts for supported Child Restraint System (CRS) sitting postures

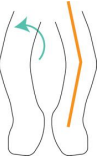

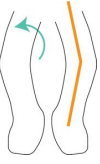

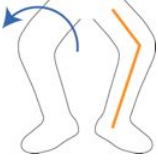

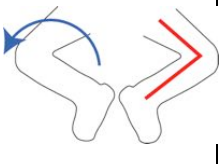

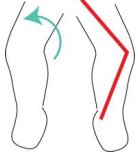

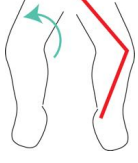

Posture	Description	Partial Illustration	Example	Count
E0	Narrow splay, obtuse knee Arms at sides			44
E1	Narrow splay, obtuse knee Arms away			33
E2	Wide splay, obtuse knee Arms away			29
E3	Wide splay, acute knee Arms away			33
E4	Narrow splay, acute knee Arms away			26
E5	Narrow splay, acute knee Arms at sides			24

Table 11. Counts for spine range of motion postures









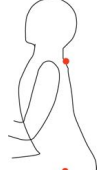

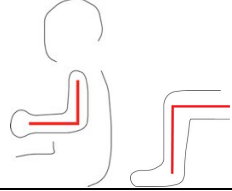

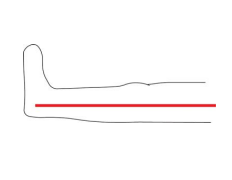

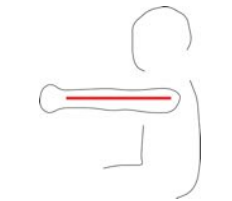

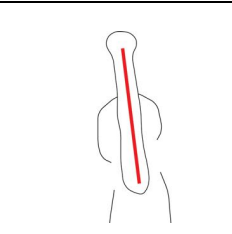

Posture	Description	Partial Illustration	Example	Count
C1	Cervical spine maximum flexion Arms away			4
V1	Natural slouch Arms away			4
V2	Entire spine in maximum flexion Arms away			26
V3	Entire spine half way flexion between V1 and V2 Arms away			9
V4	Entire spine (as much as you can safely get) in extension Arms away			13

Table 12. Counts for knee and shoulder postures

Posture	Description	Partial Illustration	Example	Count
L2	No splay, knees 90° Elbows 90°			12
LS	No splay, knee straight Elbows 90°			5
A1	Shoulder 90° flexion, Palms facing each other No splay, thigh angled down, ankle under knee			16
AY	Shoulder: ~180° flexion with arms away from head “Y”. Palms facing each other. No splay, thigh angled down, ankle under knee			15

4.3. Development of a Statistical Body Shape Model

The unsupported seated scan posture (L1) was selected for the purpose of the initial model development. The current participant pool of 47 toddlers was combined with data from 31 child participants in the Ebert et al. (2014) study to increase the overall sample size. Of these, the scans from 68 were fitted well enough to be used for the subsequent modeling. Table 13 lists summary statistics for standard anthropometric dimensions for this participant population.

Table 13. Standard Anthropometry for Combined Child Anthropometry Dataset (N=68)

Measurement	Min	Max	Mean	Percentiles				
				5th	25th	50th	75th	95th
Age (months)	11.9	58.6	31.2	13.8	21.8	27.7	40.5	55.6
Weight (kg)	9.0	23.3	13.2	9.5	11.4	12.7	14.9	17.7
Stature	710.0	1192.0	898.6	722.9	827.5	888.0	959.0	1071.8
BMI (kg/m ²)	13.6	20.7	16.3	14.0	15.2	16.1	17.3	19.1
Erect Sitting Height	442.0	680.0	530.8	460.3	497.3	527.0	558.3	603.0
Eye Height	357.0	554.0	429.0	367.2	392.0	425.0	460.0	507.0
Acromial Height	268.0	404.0	323.2	276.3	293.5	329.5	346.3	373.3
Knee Height	195.0	340.0	258.4	206.0	233.8	259.0	280.8	313.5
Shoulder-Elbow Length	133.0	239.0	173.4	136.5	156.0	168.5	188.0	219.5
Elbow-Hand Length	193.0	385.0	278.5	211.3	231.0	271.0	327.5	356.8
Buttock Knee Length	200.0	366.0	278.3	211.8	253.0	276.5	303.0	345.5
Buttock-Popliteal Length	138.0	307.0	228.5	177.8	203.8	225.5	251.5	292.0
Chest Depth (Spine)	95.0	143.0	117.4	103.0	112.0	117.5	122.8	131.8
Bispinous Breadth	97.0	216.0	123.4	107.0	114.0	121.5	130.8	143.8
Biacromial Breadth	164.0	257.0	200.1	170.4	186.0	200.0	212.0	235.6
Shoulder Breadth	196.0	300.0	235.5	205.0	216.0	235.0	248.3	281.0
Maximum Hip Breadth	137.0	243.0	185.1	162.0	172.3	185.0	197.8	214.8
Tragion to Top of Head	80.0	221.0	105.5	92.3	98.3	105.0	108.0	115.8
Head Length	141.0	193.0	167.3	153.8	161.0	167.0	173.0	181.0
Head Breadth	121.0	149.0	133.5	122.3	128.3	134.5	137.0	145.5
Chest Circumference (Axilla)	446.0	609.0	505.5	460.2	480.0	504.0	523.3	564.4
Waist Circumference	289.0	580.0	494.2	444.2	476.8	494.5	517.0	538.0
Hip Circumference (Buttocks)	450.0	620.0	517.7	465.3	491.5	517.0	535.5	568.8
Upper Thigh Circumference	236.0	383.0	295.2	240.8	277.8	294.5	311.3	341.6

A principal component analysis (PCA) was conducted to reduce the dimension of the data prior to regression analysis. A geometry vector was created for each template-fitted scan by concatenating the vertex coordinates, the landmark coordinates, and the standard anthropometric data. A PCA was conducted on the resulting geometry matrix (68 participants) and 60 principal components (PCs) were retained, representing over 99% of the variance in the data.

A regression analysis was conducted to obtain predictions of body size and shape as a function of overall characteristics. CRS occupancy specifications in the U.S. are usually based on body weight in pounds (for example, a CRS might be rated for children up to 30 lb.), body weight was a desired predictor. However, for a given body weight, shape models with both long and short torsos were also desired. Including both body weight and torso length (represented by erect sitting height) in a regression equation was problematic, because the variables are correlated in this dataset with $r=0.89$. Consequently, a PCA was conducted on the two variables to obtain two uncorrelated predictors and a linear regression analysis was conducted to predict the scores on each of the 60 PCs. The resulting PCA + regression (PCAR) model predicts child size and shape as a function of body weight and torso length (see <http://childshape.org/toddler/>).

An analysis of standard anthropometric data from Snyder et al. (1977) was conducted to establish torso length targets for each body weight of interest. Erect sitting height was used as the measure of torso length, except that for children under 24 months of age crown-rump (recumbent) length was used because erect sitting height was not available. For each body weight from 20 to 60 lb., in increments of 5 lb., data from individuals with body weight within 2.5 lb. of the target in the Snyder dataset were extracted. The number of individuals in each of these cohorts ranged from 66 to 268. The mean and standard deviation was computed for each cohort, and the 5th and 95th percentile values of torso length were computed based on a normal distribution assumption. Figure 35 shows the Snyder torso length data and lines connecting the 5th and 95th percentile values as a function of body weight.

The PCAR model was exercised for two torso lengths and nine body weights to obtain 18 body shapes. Each body shape is accompanied by predicted landmark locations and standard anthropometric variables. Note that the actual torso length in the predicted body shape does not necessarily match the target value because the scan postures are different from the standard anthropometric postures (generally more flexed, particularly for larger children). Also, the predicted anthropometric variables generated from the PCAR regression are generally slightly different from the targets due to the limitations of the regression model. Table 14 shows the input and predicted anthropometric data. Tables 15-16 show the predicted body shapes for each target body weight and torso length.

The manikins shown in Tables 15-16 are available from UMTRI in the widely used polygonal STL format (see <http://childshape.org/toddler/manikins/>). Accompanying each manikin is a text file with the 3D locations of surface landmarks associated with the manikin. The parametric model is also available online. This tool can generate for download a manikin for any combination of body weight and torso length within the range of the data.

Table 14. Target Body Dimensions for Manikins

Target Weight (lb)	Target Weight (kg)	Target Torso Length (mm)
20	9.1	443
20	9.1	509
25	11.3	480
25	11.3	550
30	13.6	512
30	13.6	580
35	15.9	541
35	15.9	615
40	18.1	567
40	18.1	640
45	20.4	598
45	20.4	668
50	22.7	619
50	22.7	692
55	24.9	641
55	24.9	713
60	27.2	655
60	27.2	730

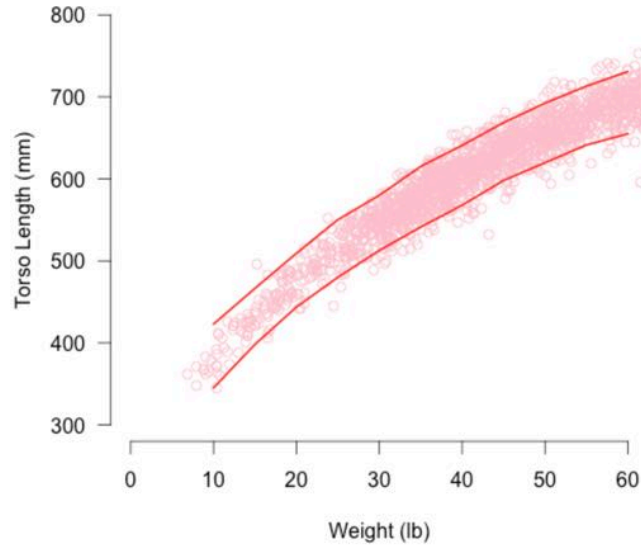
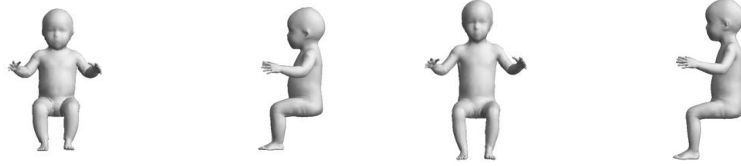


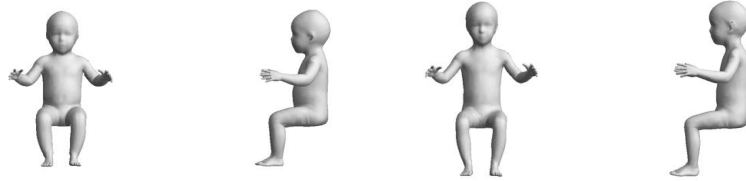
Figure 35. 5th and 95th-percentile torso lengths by body weight for children in Snyder et al. (1977).

Table 15. Front and side views of body shapes from 20 to 40 lb.



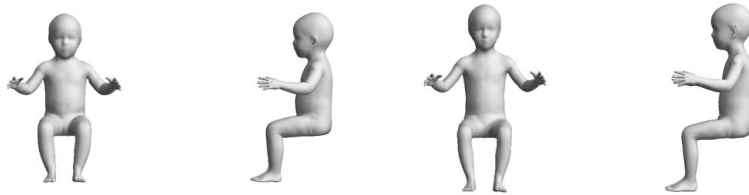
20 lb. 443 mm

20 lb. 509 mm



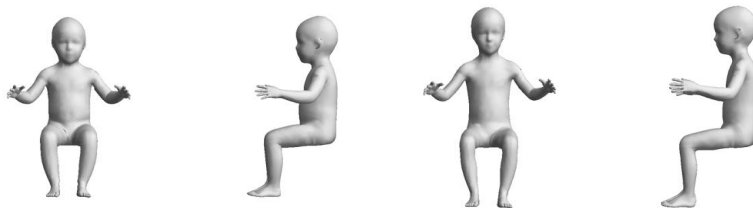
25 lb. 480 mm

25 lb. 550 mm



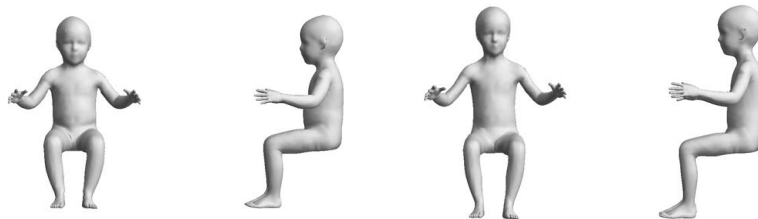
30 lb. 512 mm

30 lb. 580 mm



35 lb. 541 mm

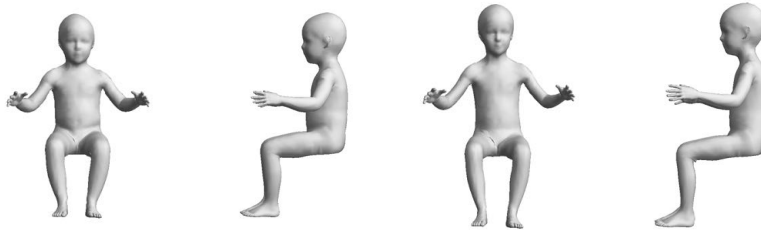
35 lb. 615 mm



40 lb. 567 mm

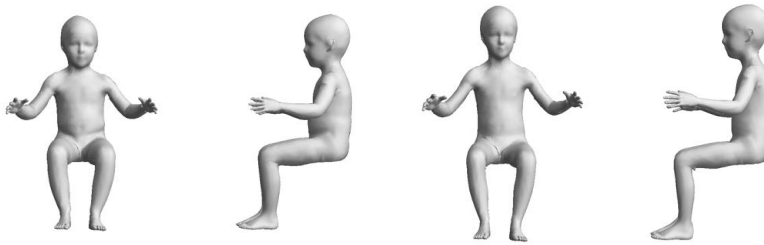
40 lb. 640 mm

Table 16. Front and side views of body shapes from 45 to 60 lb.



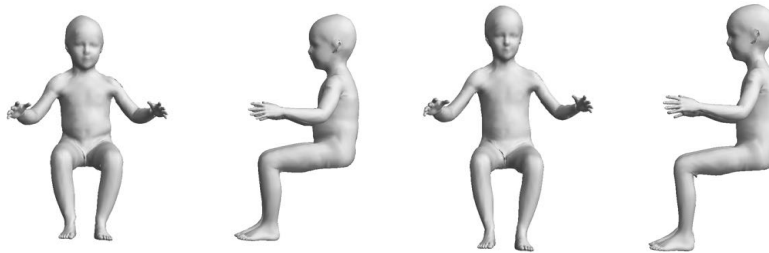
45 lb. 598 mm

45 lb. 688 mm



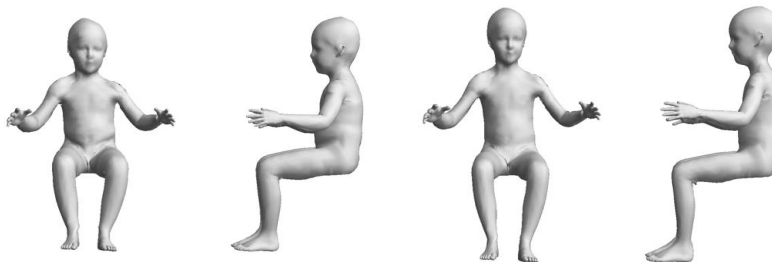
50 lb. 619 mm

50 lb. 692 mm



55 lb. 641 mm

55 lb. 713 mm



60 lb. 655 mm

60 lb. 730 mm

4.4. Example Application

The 18 manikins presented in Tables 15 and 16 represent a particular set of boundary cases that can be used to assess child restraint design. The manikins can be used to evaluate the dimensions of the restraint system, including the length of the back support, length of the seat, strap heights, and width at the shoulders. For example, if a restraint is intended for children from 20 to 40 lb., assessments could be performed with the two 20-lb manikins and the two 40-lb manikins. Accommodating these four manikins would provide good assurance that most U.S. children in the specified weight range would be accommodated.

Figures 36 through 37 show this virtual fit process schematically, using a wireframe representation of a rearward-facing child restraint system (CRS). Figure 36 shows the CRS geometry and the candidate fit model. The manikin is first centered laterally on the CRS and the buttocks are moved into position (Figure 37). The buttock area of the manikin model represents deflected flesh contours; the appropriate deformation of the padding in the CRS should be simulated by offsetting the manikin into the padding.

A virtual fit evaluation can then be performed, examining:

- top of head with respect to the top of the shell
- shoulder height relative to slots and seat back height
- shoulder breadth relative to seat interior width
- pelvis location relative to crotch portion of harness
- buttock-knee length relative to seat length
- lateral accommodation in hip area
- location of the head relative to lateral impact protection features

Because the manikin cannot currently be re-postured, interference between the extremities and the CRS geometry should generally be ignored, except that interference with the back of the calves suggests that the seat length may be too great for a child the size of the manikin.

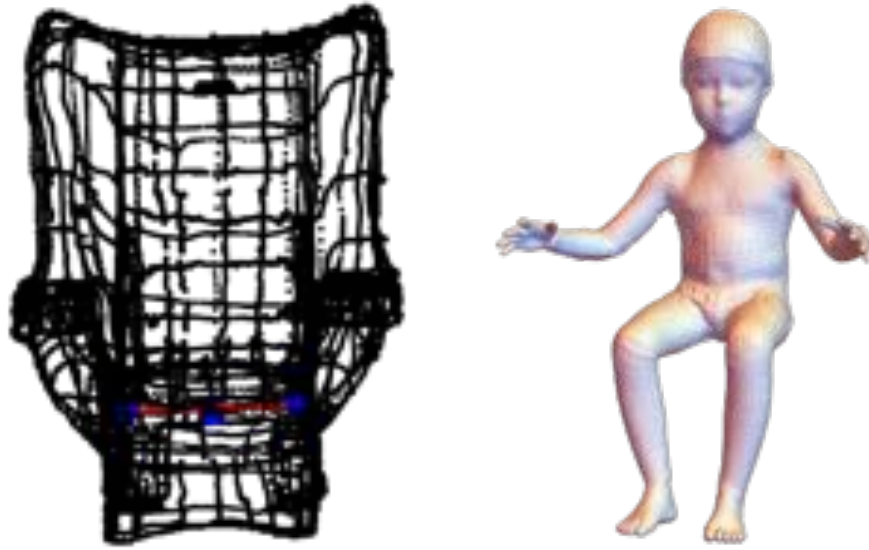


Figure 36. Wireframe representation of a child restraint and a candidate fit manikin.

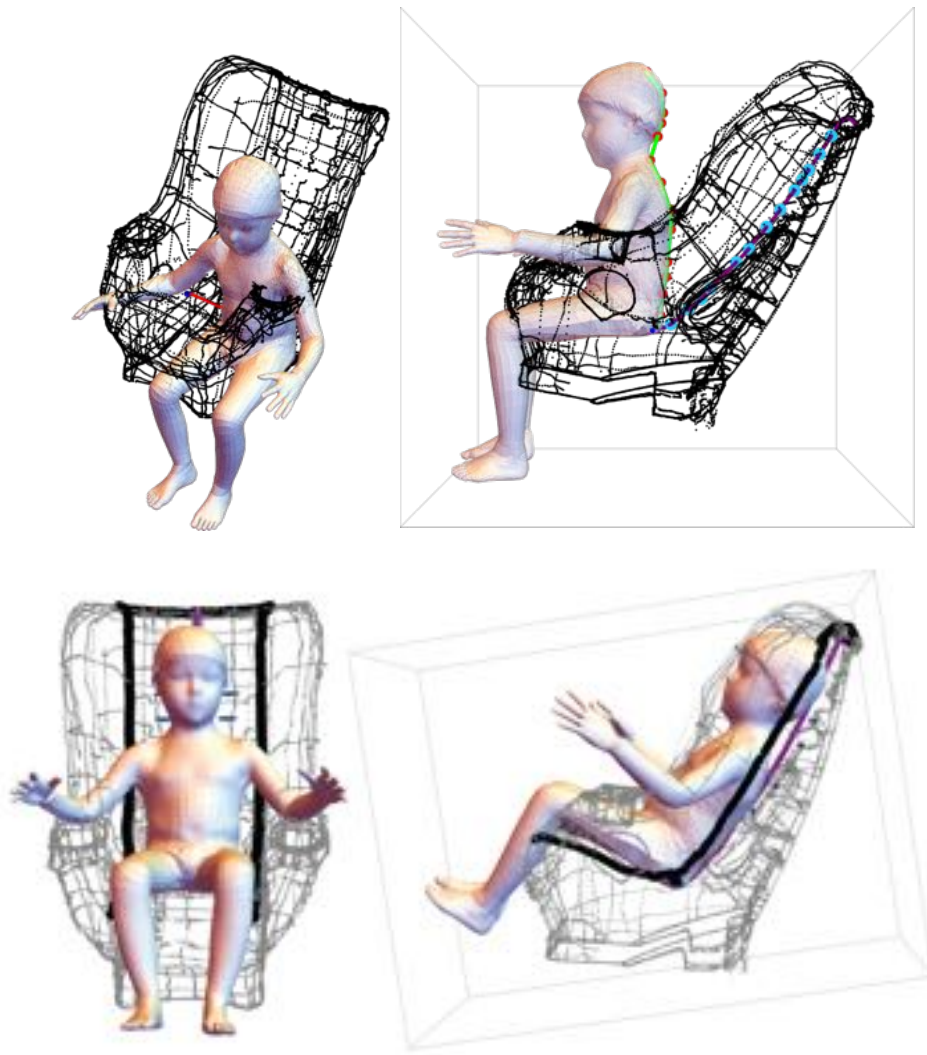


Figure 37. Aligning the manikin with the CRS geometry.

5. DISCUSSION

5.1. Accomplishments

This is the first study to quantify three-dimensional body shapes in children younger than three years of age, and the first to develop a parametric model of body shape for toddlers. The methodology followed closely the previous UMTRI development of parametric body shape models, particularly the 3- to 11-year-old model of standing children (Park and Reed 2015). However, the lack of consistency in the postures for these younger children necessitated the development of new methods for template fitting and posture standardization. The 18 manikins produced for this report are the first rigorously defined set of boundary manikins for this age cohort and are presented in a posture suitable for CRS evaluation.

5.2. Limitations and Future Work

The work is limited by the sample size. In the current study, 47 children participated, but not all were scanned in all postures. Even when combined with the data preceding study, only 68 scans in the standard seated posture were available for analysis. Due to strong correlation between overall measures of body size resulting from the large amount of growth that occurs in this age range, it is difficult to create a body shape model with more than two variables. Future studies that added to this sample would enable parameterization on additional variables such as shoulder breadth or the ratio of sitting height (torso length) to stature.

The results are limited by the characteristics of children who were measured. In particular, the results may not be representative of U.S. populations with substantial minority representation and would not be expected to accurately represent populations that are not primarily of European descent. More data will be needed to ensure representation of these populations.

The posture variability observed during scanning necessitated the development of new methods to fit the template to the scan data and to standardize the postures prior to analysis. The necessary changes in body shape associated with posture change may have introduced some errors, particularly near the hips, knees, shoulders, and elbows. However, the bootstrapping methods developed for this study had the effect of minimizing those errors. In future work, a fully posable template model is needed, along with methods for automatically “learning” the appropriate flesh deformations associated with posture changes.

The body shape modeling methods used in this study are essentially identical to those used in several previous studies of body shape (Reed and Parkinson, 2008; Park and Reed, 2015). The PCAR method produces models that show smooth, consistent variations in body shape with participant covariates such as body dimensions. However, the PCA that underlies the method is inherently linear. Each principal component is a linear combination of all of the surface mesh vertex coordinates. The linear regression predicts the principal component scores as a function of participant covariates, such as body weight. The regression models are linear in the parameters but can include nonlinear terms (such as body weight squared). For the current models, though, the effects of body weight and torso length are linear and do not interact. Hence, every vertex on the surface mesh moves the same distance and direction for a unit change in body weight or torso length regardless of the values. We might hypothesize that the effects on surface shape of a 1-lb increase in body weight for a 12-month-old child would be different than for a 36-month-old

child. However, the current sample size is not large enough to investigate those effects, so it is necessary to combine all of the data to estimate these coefficients. Due to the nature of linear regression modeling, we expect the errors to be largest at the extremes of the dataset, but methods for assessing those errors for body shape modeling are still in development. So at this time, we are unable to quantify whether the errors differ as a function of body size. In spite of these limitations, the current model represents a major advance over previous representations of child body form based on reconstructions from one-dimensional measurements.

This study gathered a large amount of data on child body shape in alternative postures that has not yet been analyzed due to resource limitations. The data quantify the effects of large ranges of upper-extremity, lower-extremity, and spine posture on body shape. This data will be useful in the development of improved ATDs as well as computational models of child occupants.

6. REFERENCES

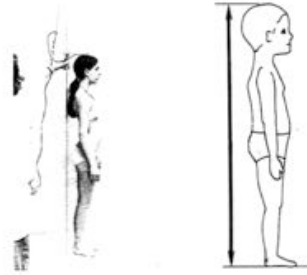
- Bland, J.M. and Altman D.G. (1986). Statistical methods for assessing agreement between two methods of clinical measurement. *Lancet* 8, 307–310.
- Ebert S.M., Klinich K.D., Manary, M.A., Malik, L.M., and Reed, M.P. (2014). Toddler Lower Extremity Posture in Child Restraint Systems. UMTRI-2014-8. University of Michigan Transportation Research Institute, Ann Arbor, MI.
- Gordon, C. C., Churchill, T., Clauser, C. E., Bradtmiller, B., McConville, J. T., Tebbetts, I., and Walker, R. A. (1989). 1988 Anthropometric Survey of U.S. Army Personnel: Methods and Summary Statistics. Final Report. (NATICK/TR-89/027). U.S. Army Natick RDEC.
- Horn, B. K. P. (1987). Closed-form solution of absolute orientation using unit quaternions. *Journal of the Optical Society of America*, 4(4), 629-642.
- Humbert, M., Gey, N., Muller, J., & Esling, C. (1996). Determination of a Mean Orientation from a Cloud of Orientations. Application to Electron Back-Scattering Pattern Measurements. *Journal of Applied Crystallography*, 29(6), 662-666.
- Irwin, A.L, and Mertz, H.J. (1997). Biomechanical bases for the CRABI and Hybrid III child dummies. *Proceedings of the 41st Stapp Car Crash Conference*. SAE International, Warrendale, PA.
- Klinich, K. D., Boyle K., Malik, L, Manary, M. Hu, J. (2015). Installed Positions of Child Restraint Systems in Vehicle Second Rows. SAE Technical Paper 2015-01-1452.
- Manary, M.A., Klinich, K.D., Orton, N.R., Reed, M.P., Rupp, J.D. (2013). Comparing the CRABI-12 and CRABI-18 for Infant Child Restraint System Evaluation. UMTRI Technical Report 2013-31.
- Pagano, B., Parkinson, M.B., and Reed, M.P. (2015). An updated estimate of the body dimensions of U.S. children. *Ergonomics*. 58(6):1045-57. 10.1080/00140139.2014.1000392.
- Park, B-K and Reed, M.P. (2015). Parametric body shape model of standing children ages 3 to 11 years. *Ergonomics*. 10.1080/00140139.2015.1033480
- Reed, M.P., Lehto, M.M., Schneider, L.W., Moss, S., Nghi, T. (2001). Development of anthropometric specifications for the six-year-old OCATD. *SAE Transactions: Journal of Passenger Cars — Mechanical Systems*, 110: 497-504.
- Reed, M.P., Ebert-Hamilton, S.M., Manary, M.A., Klinich, K.D., and Schneider, L.W. (2005). A new database of child anthropometry and seated posture for automotive safety

- applications. SAE Transactions: Journal of Passenger Cars - Mechanical Systems, 114: 2222-2235.
- Reed, M.P., Manary, M.A., and Schneider, L.W. (1999). Methods for measuring and representing automobile occupant posture. Technical Paper 990959. Society of Automotive Engineers, Warrendale, PA.
- Reed, M.P., Ebert-Hamilton, S.M., Klinich, K.D., Manary, M.A., and Rupp, J.D. (2013). Effects of vehicle seat and belt geometry on belt fit for children with and without belt positioning booster seats. *Accident Analysis and Prevention*. 50:512-22. 10.1016/j.aap.2012.05.030
- Reed, M.P., Ebert-Hamilton, S.M., Manary, M.A., Klinich, K.D., and Schneider, L.W. (2006). Improved positioning procedures for 6YO and 10YO ATDs based on child occupant postures. *Stapp Car Crash Journal*, 50: 337-388.
- Reynolds, H. M., Young, J. W., McConville, J. T., and Snyder, R. G. (1976). Development and evaluation of masterbody forms for three-year old and six-year old child dummies. Final Report No. DOT/HS 801 811. Washington, D.C.: National Highway Traffic Safety Administration.
- Snyder, R.G., Schneider, L.W., Owings, C.L., Reynolds, H.M., Golumb, D.H., and Schork, M.A. (1977). Anthropometry of Infants, Children, and Youths to Age 18 for Product Safety Design. Final Report UM-HSRI-77-17. University of Michigan Transportation Research Institute, Ann Arbor, MI.
- Weber, K.W., Lehman, R.J., and Schneider, L.W. (1985). Child Anthropometry for Restraint System Design. UMTRI Technical Report 85-23. University of Michigan Transportation Research Institute, Ann Arbor, MI.

APPENDIX A
Standard Anthropometric Measures

Stature Standing(Snyder)

Subject stands erect with head oriented in the Frankfort Plane (tragion to infraorbitale level), arms hanging at sides. With an anthropometer, measure the vertical distance from the standing surface to vertex (top of the head).



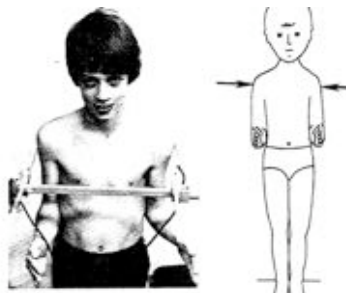
Crown-Sole Length Supine (Snyder)

Subject lies on back with legs extended; the head is aligned in the Frankfort Plane relative to the extended torso. Measure the parallel distance from vertex to the heel of the right foot with an anthropometer. An assistant is required to assure that the subject is in the correct position.



Shoulder Breadth (Snyder)

Subject stands erect, upper arm at sides, and elbows flexed 90°. With the paddle blades of an anthropometer, measure the horizontal breadth across the shoulders.



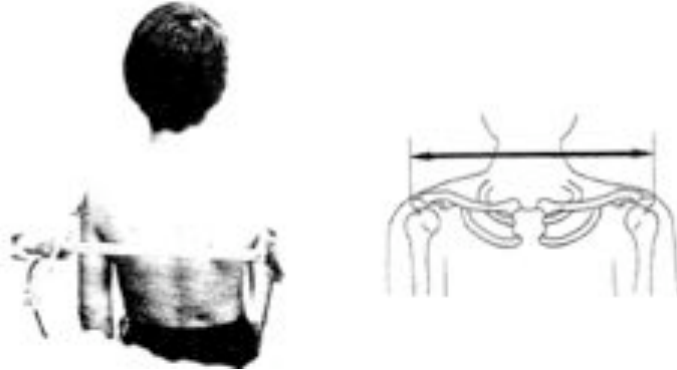
Shoulder Breadth Supine (Snyder)

Subject lies on back with arms held at side. Measure the maximum horizontal breadth across the shoulders with an anthropometer. Pressure is momentarily applied with the pressure-transducer paddle-blade. An assistant is required to assure that the subject is in the correct position.



Biacromial Breadth (Snyder)

Subject stands erect, arms hanging at sides. With the pointed blades of the anthropometer, measure the horizontal distance between the most lateral edges of the right and left acromion landmarks. *(Make sure shoulders are in widest position)*

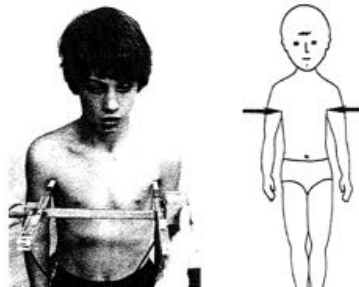


Biacromial Breadth Supine

Subject lies on back, arms held at sides. With the pointed blades of the anthropometer, measure the horizontal distance between the most lateral edges of the right and left acromion landmarks. *(Make sure shoulders are in widest position)*

Chest Breadth

Subject stands erect with feet together, weight evenly distributed, arms initially raised then lowered when instrument is in place with the pointed blades of an anthropometer, measure the horizontal breadth of the chest at the level of the axilla (armpit).



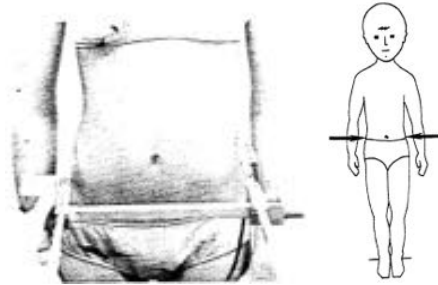
Chest Breadth Supine

Subject lies on back. Measure the horizontal breadth of the chest at the level of the nipples with an anthropometer. Pressure is momentarily applied with the paddle-blade. An assistant is required to assure that the subject is in the correct position.



Waist Breadth Omphalion (Snyder)

Subject stands erect with feet together, weight evenly distributed. With the paddle blades of an anthropometer, measure the horizontal breadth of the torso at the level of the umbilicus (navel).



Waist Breadth Omphalion Supine

Subject lies on back. With the paddle blades of an anthropometer, measure the horizontal breadth of the torso at the level of the umbilicus (navel).

Waist Depth (Omphalion)

Subject stands erect, upper arms hanging at sides. With the paddle blades of an anthropometer, measure the horizontal depth of the torso at the level of the umbilicus (navel).

Waist Depth Supine (Omphalion)

Subject lies on back with 90° right hip flexion and 90° right knee flexion. Measure the parallel distance from surface on which the subject is lying to the right of the umbilicus (navel).

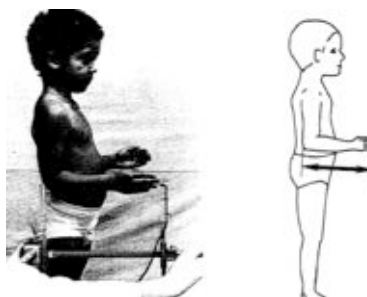
Shoulder-Elbow Length (Snyder)

Subject stands erect, upper arms hanging at sides and elbows flexed 90°. With the paddle blades of an anthropometer, measure the distance from the superior surface of the right shoulder to the inferior surface of the forearm just below the elbow parallel to the long axis of the upper arm.



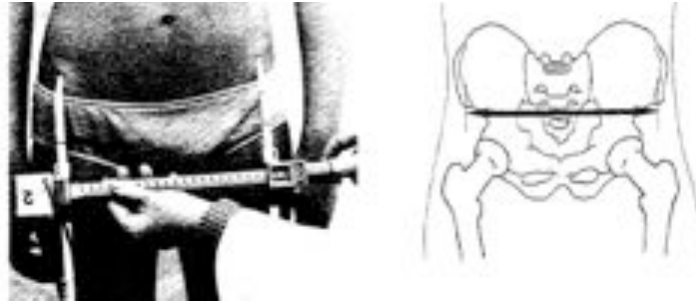
Elbow- Hand Length (Snyder)

Subject stands erect, upper arms hanging at sides and elbows flexed 90° with hands and fingers extended. With the paddle blades of an anthropometer, measure the distance from the posterior surface of the right upper arm just above the elbow to the tip of the middle finger parallel to the long axis of the forearm.



Bispinous Breadth (Snyder)

Subject stands erect with feet together, weight evenly distributed. With the pointed blades of an anthropometer, measure the distance between the right and left anterior superior iliac spines of the pelvis.



Pelvic Breadth

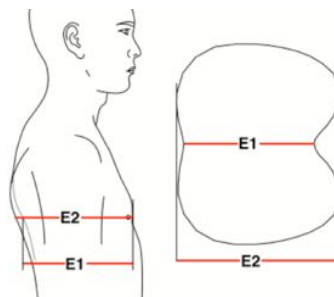
Subject stands erect. With the blades of an anthropometer, measure the distance between the right and left ilioacristale of the pelvis. Flesh is firmly compressed.

Pelvic Depth (ASIS-PSIS)

Subject stands erect. With the blades of an anthropometer, measure the distance between the right ASIS and PSIS of the pelvis. Flesh is firmly compressed.

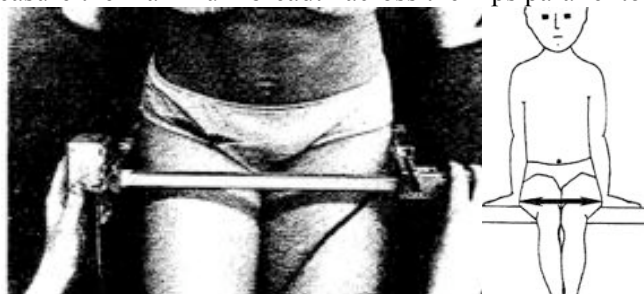
Chest Depth (on spine) – (E1 in illustration)

The horizontal distance between the sternum, at the level of the right bust point on women or the nipple on men (*and children*), and the spine at the same level is measured with a curved caliper. The subject stands erect looking straight ahead. The shoulders and upper extremities are relaxed. The measurement is taken at the maximum point of quiet respiration.



Maximum Hip Breadth (Snyder)

Subject sits erect with knees together, feet resting on a platform adjusted for 90° knee flexion. With the paddle blades of an anthropometer, measure the maximum breadth across the hips parallel to the seated surface.

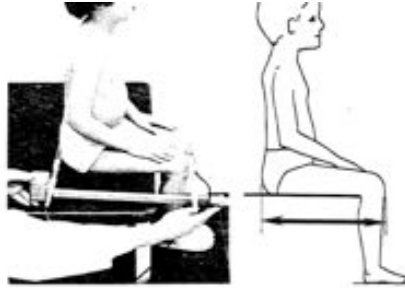


Maximum Hip Breadth Supine

Subject lies on back with knees together, lower legs resting on a platform adjusted to achieve 90° knee flexion and 90° hip flexion. With the paddle blades of an anthropometer, measure the maximum breadth across the hips perpendicular to midsagittal plane.

Buttock-Knee Length (Snyder)

Subject sits erect, feet resting on a platform adjusted for 90° knee flexion. With the paddle blade of an anthropometer, measure the distance from the posterior surface of the right buttock to the anterior surface of the knee parallel to the long axis of the upper leg.



Buttock-Knee Length Supine (adapted from Snyder)

Subject lies on back with 90° right hip flexion and 90° right knee flexion. Measure the parallel distance from surface the buttocks is resting on to the anterior surface of the right knee with an anthropometer. An assistant is required to assure that the subject is in the correct position.



Buttock-Popliteal Length (ANSUR)

The horizontal distance between a buttock plate placed at the most posterior point on either buttock and the back of the right knee (the popliteal fossa at the dorsal juncture of the calf and thigh) is measured with an anthropometer. The subject sits erect. The thighs are parallel and the knees flexed 90° with the feet in line with the thighs.

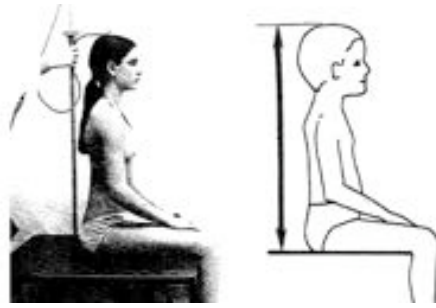


Buttock-Popliteal Length Supine

Subject lies on back with 90° right hip flexion and 90° right knee flexion. Measure the parallel distance from surface the buttocks is resting on back of the right knee (the popliteal fossa at the dorsal juncture of the calf and thigh) is measured with an anthropometer. An assistant is required to assure that the subject is in the correct position.

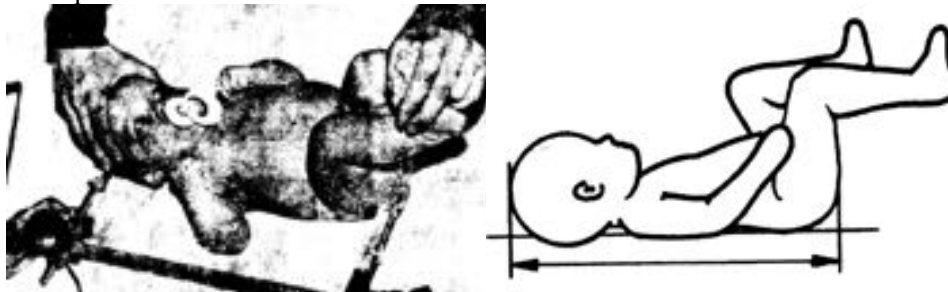
Erect Sitting Height (Snyder)

Subject sits erect with head oriented in the Frankfort Plane (tragion to infraorbitale level), arms hanging at sides, hands resting on thigh. With the paddle blade of the anthropometer, measure the vertical distance from the sitting surface to the vertex (top of head).



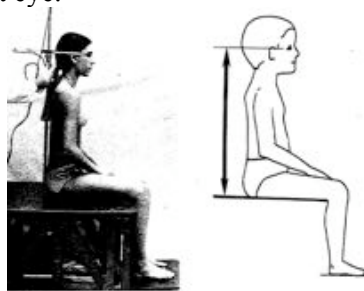
Crown-Rump Length (Snyder)

Subject lies on back with leg flexed 90° to torso so that rotation of the pelvis is minimal. Measure the parallel distance from vertex to the surface of the right buttock with an anthropometer. Pressure is momentarily applied with the pressure transducer paddle-blade on the interior surface of the buttock. An assistant is required to assure that the subject is in the correct position.



Eye Height Sitting (Snyder)

Subject sits erect with head oriented in the Frankfort Plane (tragion to infraorbitale level), arms hanging at sides. With the pointed blade of the anthropometer, measure the vertical distance from the sitting surface to the outer external canthus (outer corner) of the right eye.



Eye-Rump Height Supine

Subject lies on back with leg flexed 90° to torso so that rotation of the pelvis is minimal and Frankfort Plane Vertical. Measure the parallel distance from outer external canthus (outer corner) of the right eye to the surface of the right buttock with an anthropometer. Pressure is momentarily applied with the pressure transducer paddle-blade on the interior surface of the buttock. An assistant is required to assure that the subject is in the correct position.

Seated Shoulder Height (ANSUR)

The vertical distance between a sitting surface and the lateral anterior margin of the acromion is measured with an anthropometer. The subject sits erect looking straight ahead. The shoulders and upper arms are relaxed and the forearms and hands are extended forward horizontally with the palms facing each other. The measurement is made at the maximum point of quietest respiration.

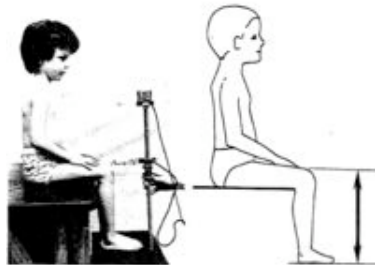


Shoulder-Rump Height Supine (Snyder)

Subject lies on back with leg flexed 90° to torso so that rotation of the pelvis is minimal. The vertical distance between the right buttocks and the lateral anterior margin of the acromion is measured with an anthropometer. The shoulders and arms are relaxed by the side of the subject.

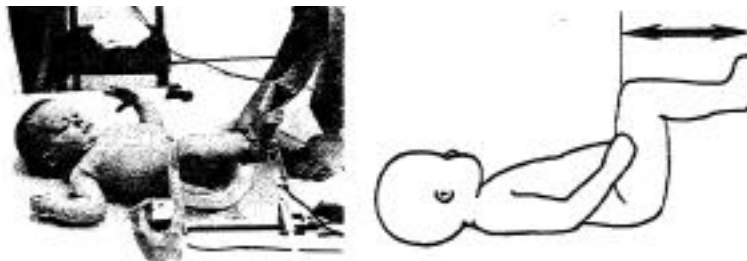
Knee Height (Snyder)

Subject sits erect, feet resting on a platform adjusted for 90° knee flexion. With the paddle blade of an automated anthropometer, measure the vertical distance from the foot-resting surface to the top of the right knee, just in back and above the patella (knee cap).



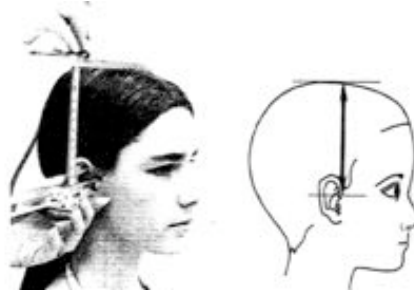
Knee-Sole Length Supine (Snyder)

Subject lies on back with the right knee flexed 90°. With the paddle blades of an anthropometer, measure the distance from the superior surface of the right knee to the heel of the right foot. An assistant is required to assure that the infant's in the correct position.



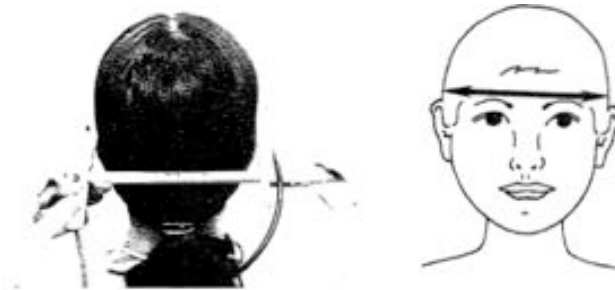
Tragion to Top of Head (Snyder)

Subject sits erect with head oriented in the Frankfort Plane. With the pointed blades of a sliding caliper, measure the vertical distance from tragion to vertex.



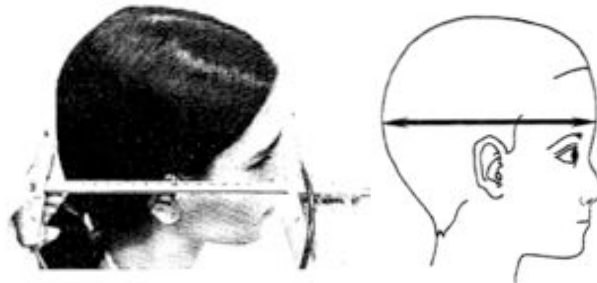
Head Breadth (Snyder)

Subject sits erect with head oriented in the Frankfort Plane, arms hanging at sides. With the paddle blades of the sliding caliper, measure the maximum breadth of the head above and behind the ears.



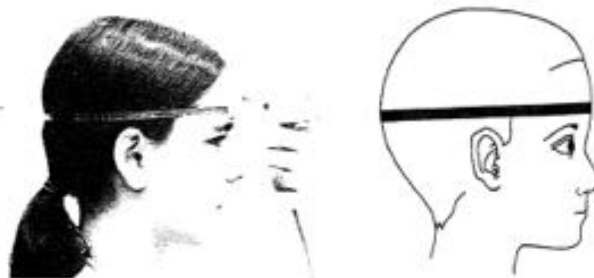
Head Length (Snyder)

Subject stands erect with head oriented in the Frankfort Plane. With the paddle blades of an anthropometer or slide caliper, measure the distance from the glabella (most anterior protrusion of the forehead) to opithocranium (most posterior point from glabella on the back of the head).



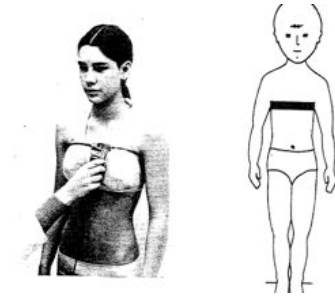
Head Circumference (Snyder)

Subject stands erect, arms hanging at sides. With an automated tape device, measure the circumference of the head at the level of the plane passing above glabella (most anterior protrusion of forehead) and through opithocranium (most posterior protrusion from glabella on the back of the head), perpendicular to the mid-sagittal plane.



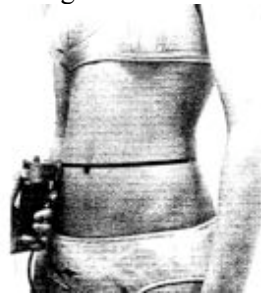
Chest Circumference at Axilla (Snyder)

Subject stands erect, arms initially raised, then lowered when tape is in place. With a tape device, measure the horizontal circumference of the chest during normal breathing at the level of the axilla (armpit).



Waist Circumference (Snyder)

Subject stands erect with feet together, weight evenly distributed and arms hanging at sides. With a tape device, measure the horizontal circumference of the waist during normal breathing at the level of the umbilicus (navel).



Hip Circumference at Buttocks (Snyder)

Subject stands erect with feet together, weight evenly distributed and arms hanging at sides. With a tape device, measure the horizontal circumference of the hips at the level of the greatest posterior protrusion of the buttocks, as viewed from the side.



Upper Thigh Circumference (Snyder)

Subject stands erect with legs slightly separated, weight evenly distributed. With a tape device, measure the horizontal circumference of the right thigh at the level of the gluteal furrow.



Maximum Calf Circumference (Snyder)

Subject sits with right leg extended and relaxed. Measure the maximum horizontal circumference at the level of the greatest posterior protrusion of the calf with an automated tape device that applies constant tension.



Maximum Calf Circumference Supine (Snyder)

Subject lies on back with right leg extended and supported free of surface. Measure the maximum horizontal circumference at the level of the greatest posterior protrusion of the calf with a tape device that applies constant tension. An assistant is required to assure that the subject is in the correct position.



Ankle Circumference (Snyder)

Subject sits with right leg extended and relaxed. Measure the minimum horizontal circumference of the ankle above the malleoli with a tape device that applies constant tension.



Ankle Circumference Supine (Snyder)

Subject lies on back with right leg extended and supported free of crib surface. Measure the minimum horizontal circumference of the ankle above the malleoli with a tape device that applies constant tension. An assistant is required to assure that the subject is in the correct position.



Upper Arm Circumference (Snyder)

Subject sits erect with right arm extended. Measure the circumference perpendicular to the long axis of the limb midway between the shoulder and elbow with an automated tape device that applies a constant tension.



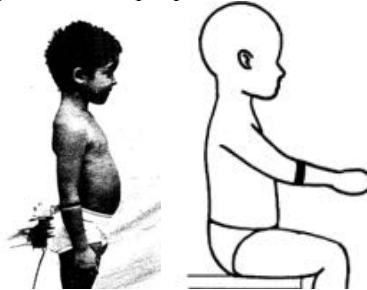
Upper Arm Circumference Supine (Snyder)

Subject lies on back with right arm extended. Measure the circumference perpendicular to the long axis of the limb midway between the shoulder and elbow with an automated tape device that applies a constant tension.



Maximum Forearm Circumference (Snyder)

Subject stands erect, arms hanging at sides. (or sits erect with arm extended) With an automated tape device, measure the maximum circumference of the right forearm perpendicular to the long axis of the limb.



Maximum Forearm Circumference Supine (Snyder)

Subject lies on back with right arm extended. Measure the maximum circumference perpendicular to the long axis of the limb with a tape device that applies constant tension. An assistant is required to assure that the infant is in the correct position.



Definitions

Acromion – The most lateral bony point on the acromion process of the scapula (shoulder blade). It is near the shoulder joint center of rotation.

Axilla – the armpit

Bustpoint – the anterior punt of the bra cup

Glabella – The most prominent point palpable on the forehead between the eyebrows (Supra-orbital ridges) and above the junction of the nose (nasofrontal suture) with the forehead.

Iliocristale – The highest point on the lateral brim of the iliac crest of the pelvis.

Gluteal furrow point – the lowest point of the lowest furrow or crease at the juncture of the right buttock and the thigh.

APPENDIX B

Points Digitized on Scans

Table B1a. Markers Digitized on Scans

Marker Name	Body Part	Description
AcromionLt H	Torso	
AcromionRt H	Torso	
ElbowMedLt M	Arm	Medial epicondyle (marked with elbow bent 45°) (inside of elbow) , Left
ElbowMedRt M	Arm	Medial humeral epicondyle (mark with elbow bent 45°), Right
ElbowLatLt M	Arm	Lateral epicondyle (mark with elbow bent 45°) (outside of elbow) , Left
ElbowLatRt M	Arm	Lateral humeral epicondyle (mark with elbow bent 45°), Right
SpineC07 M	Torso	Spinous process of the 7th cervical vertebra (cervicale)
SpineT04 M	Torso	Spinous process of 4th thoracic vertebra
SpineT08 M	Torso	Spinous process of 8th thoracic vertebra
SpineT12 M	Torso	Spinous process of 12th thoracic vertebra
SpineL03 M	Torso	Spinous process of 3rd lumbar vertebra
SternSup22Y18ZLt M	Torso	Marker 18 mm down and 22 to left of suprasternale, Left
SternSub22Y18ZRt M	Torso	Marker 18 mm down and 22 to right of suprasternale, Right
SternSup60ZCt M	Torso	Marker 60 mm down from suprasternale
IlioLt M	Torso	Marker on Iliocristale (most superior lateral point on pelvis) , Left
IlioRt M	Torso	Marker on Iliocristale (most superior lateral point on pelvis) , Right
KneeFemMedLt M	Leg	Femoral epicondyle, medial, Left
KneeFemMedRt M	Leg	Femoral epicondyle, medial, Right
KneeFemLatLt M	Leg	Femoral epicondyle, lateral, Left
KneeFemLatRt M	Leg	Femoral epicondyle, lateral, Right
AnkleLatLt M	Leg	Malleolus, lateral, Left
AnkleLatRt M	Leg	Malleolus, lateral, Right
AnkleMedLt M	Leg	Malleolus, medial, Left
AnkleMedRt M	Leg	Malleolus, medial, Right

Table B1b. Landmarks Digitized on Scans

Point Name	Body Part	Additional Description
HeadTopCt_L	Head	Most superior point on head or helmet
HeadBackCt_L	Head	Most posterior point on head or helmet
HeadTragLt_L	Head	Notch just above the tragus of the ear
EyeCorLt_L	Head	Point on orbit nearest the corner of eye
EyeCenLt_L	Head	Point on orbit below the eye at the same lateral position as the pupil when looking straight forward
HeadGlabCt_L	Head	Glabella: Smooth elevation of the frontal bone just above the bridge of the nose, between eyebrows
EyeCenRt_L	Head	Point on orbit below the eye at the same lateral position as the pupil when looking straight forward
EyeCorRt_L	Head	Point on orbit nearest the corner of eye
HeadTragRt_L	Head	Notch just above the tragus of the ear
NoseTipCt_L	Head	Tip of nose
ChinTipCt_L	Head	Menton (tip of chin)
WristLatLt_L	Arm	Styloid process on ulna (pinky side) – opposite of wrist “bump”
WristLatRt_L	Arm	Styloid process on ulna (pinky side) lateral point on wrist “bump”
WristMedLt_L	Arm	Styloid process on radius (thumb side) – opposite of wrist “bump”
WristMedRt_L	Arm	Styloid process on radius (thumb side) lateral point on wrist “bump”
Mcar5LatRt_L	Arm	Knuckle – grip axis, pinky side (5 th metacarpal medial)
Mcar2MedRt_L	Arm	Knuckle – grip axis, index side
Mcar2MedLt_L	Arm	Knuckle – grip axis, pinky side
Mcar5LatLt_L	Arm	Knuckle – grip axis, index side
SternSupCt_L	Torso	Anterior surface of jugular notch
SternSubCt_E	Torso	Substernale
InnerThighCt_E	Torso	Most inferior midline point on torso – mid crotch point
ThighJnctRtLat_L	Torso	Thigh – abdominal junction, lateral point (defining a line)
ThighJnctRtMed_L	Torso	Thigh – abdominal junction, medial point (defining a line)
ThighJnctLtMed_L	Torso	Thigh – abdominal junction, medial point (defining a line)
ThighJnctLtLat_L	Torso	Thigh – abdominal junction, lateral point (defining a line)
AxillaLtFt_L	Torso	Armpit Front (anatomical – not where the scan separates)
AxillaRtFt_L	Torso	Armpit Front
AxillaRtRr_L	Torso	Armpit Rear
AxillaLtRr_L	Torso	Armpit Rear
CenterButtocks_E	Torso	Most posterior midline point on the buttocks
FootMtar5LatLt_L	Leg	Ball of foot lateral (metatarsal-phalangeal protrusion)
FootMtar5LatRt_L	Leg	Ball of foot lateral
FootMtar1MedLt_L	Leg	Ball of foot medial
FootMtar1MedRt_L	Leg	Ball of foot medial
FootToe1Lt_L	Leg	Acropodian (most distal phalangeal point)
FootToe1Rt_L	Leg	Acropodian (most distal phalangeal point)
FootHeelRt_L	Leg	Most posterior point on right heel
FootHeelLt_L	Leg	Most posterior point on left heel
KneeSupLt_L	Leg	Most proximal point on left patella
KneeInfLt_L	Leg	Most distal point on left patella
KneeSupRt_L	Leg	Most proximal point on right patella
KneeInfRt_L	Leg	Most distal point on right patella

Table B2. Seat Hardware Digitized on Scans

Corners of seat pan frame	Corners of Footrest Surface
SeatTop_Rr_Lt_S	FootBlocks_TpRr_Rt_S
SeatTop_Ft_Lt_S	FootBlocks_BtRr_Rt_S
SeatTop_Rr_Rt_S	FootBlocks_BtRr_Lt_S
SeatTop_Ft_Rt_S	
Corners of seat back surface	Reference Marks on CRS Frame
SeatBack_Tp_Lt_S	CRSRef_BackTop_Lt_S
SeatBack_Bt_Lt_S	CRSRef_BackBot_Lt_S
SeatBack_Tp_Rt_S	CRSRef_PanFt_Lt_S
SeatBack_Bt_Rt_S	CRSRef_Frm_Lt_S

APPENDIX C

Comparison of Standard Anthropometric Measures Across Postures

Standard anthropometric were taken in multiple posture (standing, seated, and supine) when possible to provide preliminary data on how these anthropometric measures vary with posture. Agreement between the standard anthropometric dimensions recorded in different postures was assessed following the Bland and Altman (1986) method. Differences in the traditional anthropometry measures recorded from two postures were tested for normality using the Shapiro-Wilk W Test. With the exception of stature, all of the measures were normally distributed. Plots of the difference between anthropometric measures in two postures against the mean of the two measures were performed for each dimension. Accuracy and agreement was assessed by calculating the bias (mean difference and standard deviation of the differences). Bias, 95% confidence intervals for the bias, and 95% limits of agreement (bias \pm 2SD) for anthropometric measures were detailed in Table 1.

Figure C1 demonstrates the considerable lack of agreement between the standing and supine measures of stature, with discrepancies up to 150 mm. These differences exceed the limits of agreement (-15.6 ± 65.6 mm) and caution that measures of stature in the standing and supine postures cannot be used interchangeably. The mean difference is 15.6 mm (with 95% confidence interval -5.5 to -25.7 mm. For the toddler participant pool, bideltoid breadth (standing-supine), bideltoid breadth (sitting-supine), waist breadth, and knee height dimensions showed a nonstatistical mean difference (Table C1, Figure C2). The remaining anthropometric measures did not demonstrate a good agreement between measures acquired from the two postures (Figure C3-C4).

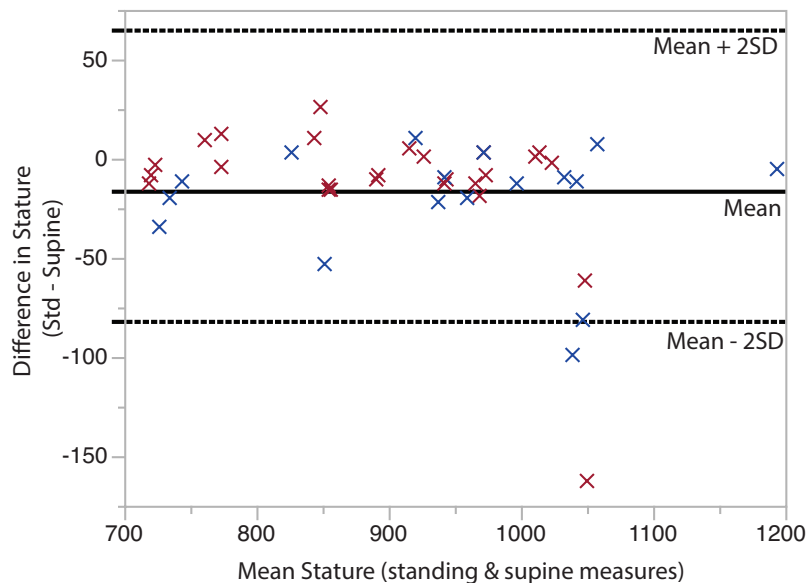


Figure C1. Comparison of stature dimension (mm) between measures recorded in standing and supine postures by Bland and Altman (1986) plots. Central line (solid black) represents mean difference (bias) between two postures. Mean \pm 2SD lines (dashed) represent upper and lower limits of agreement. Female and males are denoted by red and blue markers.

Dimension	Posture	N	Bias (mean)	95% CI (Bias)	95% Limits of Agreement	Normality Assumption	Prob > t
Stature	Std-Supine	43	-15.6	± 10.1	± 65.6	0.0001	0.0032
Erect Seated Height	Sit-Supine	42	-34.1	± 5.6	± 35.8	0.1283	<.0001
Seated Eye Height	Sit-Supine	37	-28.4	± 9.2	± 55.2	0.2783	<.0001
Seated Shoulder Height	Sit-Supine	39	-64.3	± 9.0	± 55.7	0.2662	<.0001
BiDeltoid Breadth	Std-Supine	22	-3.6	± 5.2	± 23.4	0.2466	0.1592
BiDeltoid Breadth	Sit-Supine	11	-1.2	± 8.3	± 24.7	0.2795	0.7577
Waist Breadth	Std-Sit	35	-1.7	± 3.2	± 18.4	0.0426	0.287
Hip Breadth	Sit-Supine	38	5.1	± 4.1	± 25.1	0.0017	0.0174
Buttock-Knee Length	Sit-Supine	41	18.0	± 5.3	± 33.6	0.0529	<.0001
Buttock-Popliteal Length	Sit-Supine	40	16.5	± 5.4	± 33.7	0.1584	<.0001
Knee Height	Sit-Supine	40	2.6	± 2.9	± 18.3	0.0984	0.0821

Table C1. Bias and 95% limits of agreement for standard anthropometric measures (standing, sitting, supine).

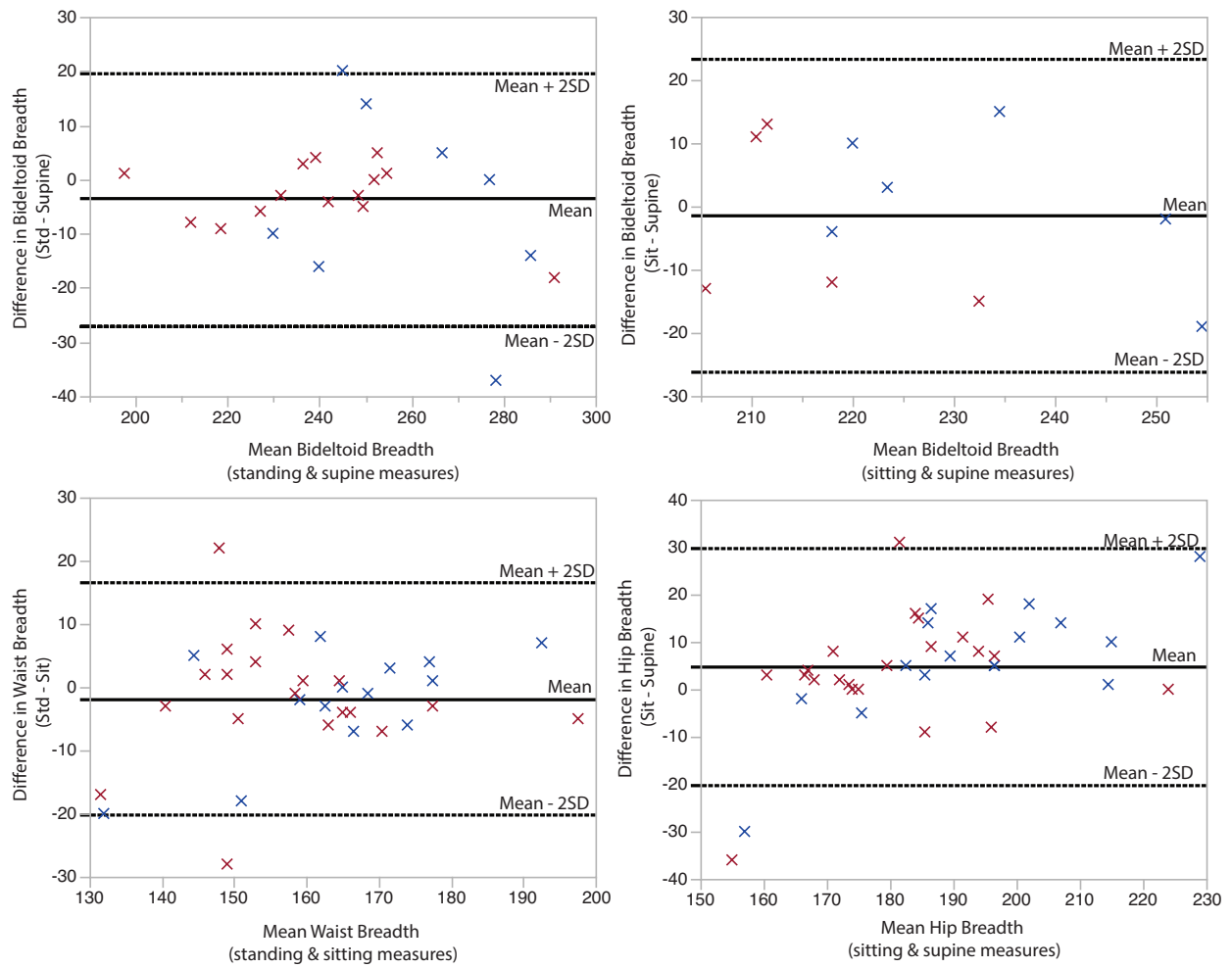


Figure C2. Comparison of bideltoid breadth, waist breadth, and hip breadth dimensions (mm) between measures recorded in standing and supine, and sitting and supine postures.

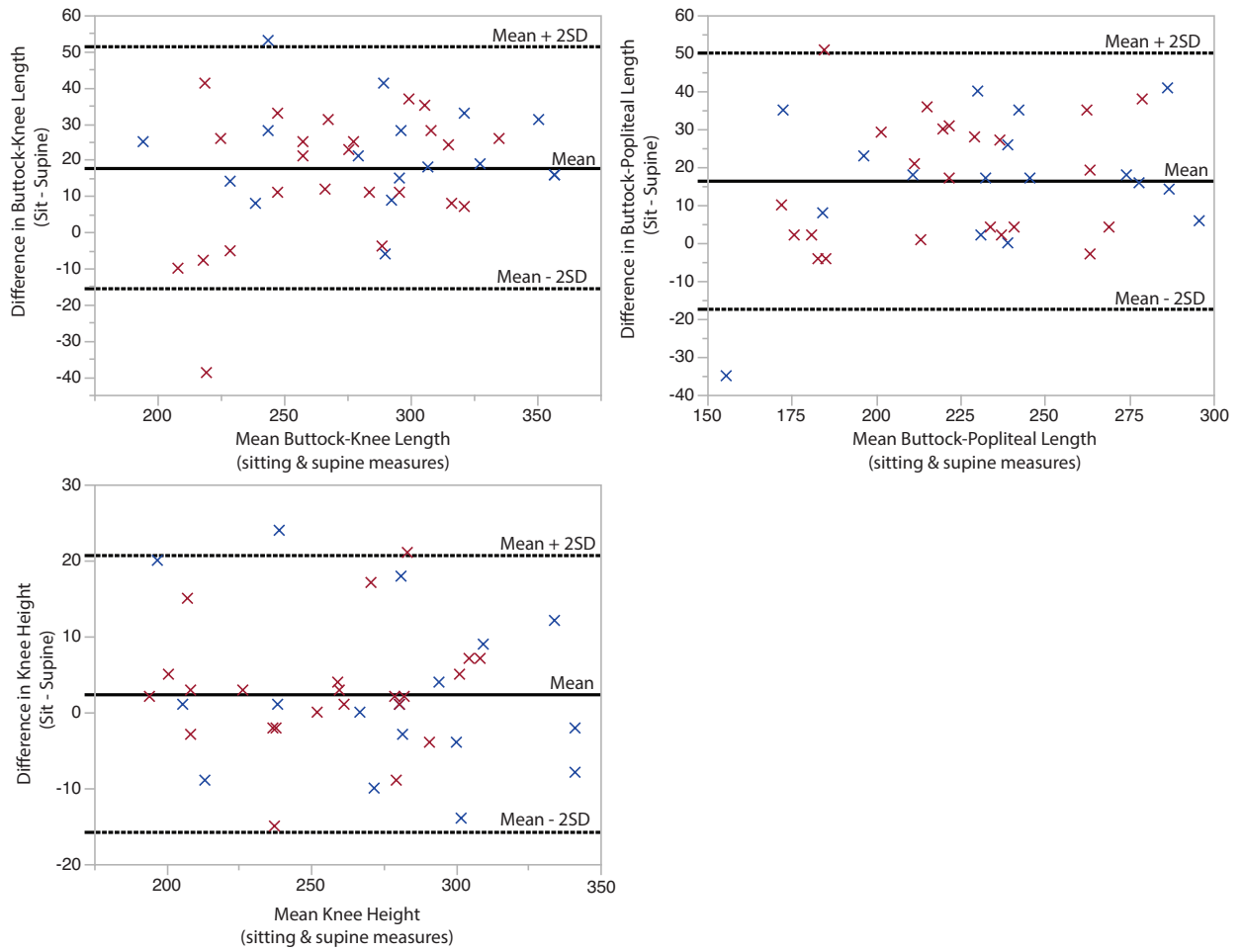


Figure C3. Comparison of buttock-knee and buttock-popliteal lengths and knee height dimensions (mm) between measures recorded in sitting and supine postures.

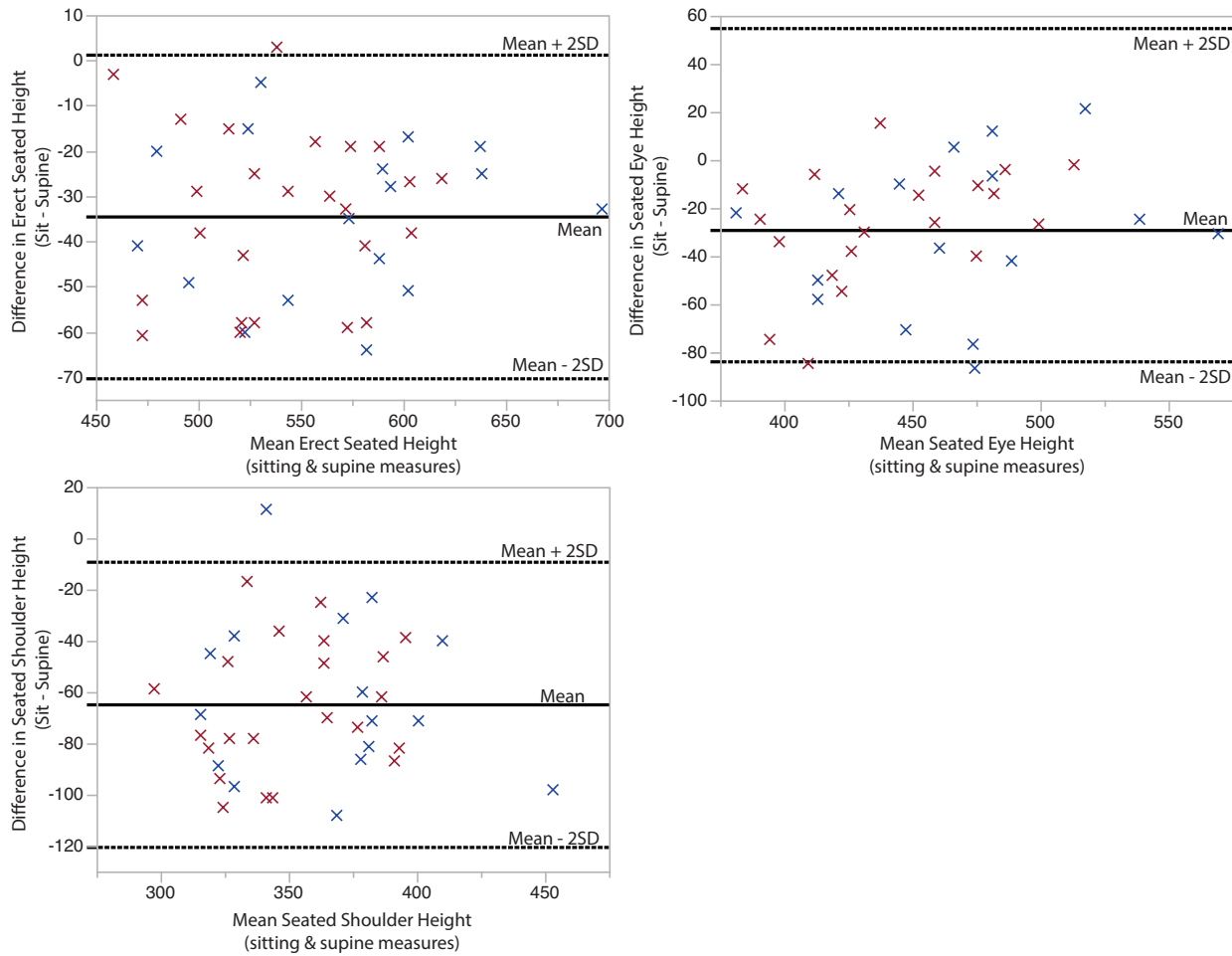


Figure C4. Comparison of erect seated height, seated eye height and seated shoulder height dimensions (mm) between measures recorded in sitting and supine postures.